CERTIFICATE

This is to certify that The Thesis titled, **"DETERMINATION OF FRACTURE CHARACTERISTICS OF NUCLEAR WELD USING MODIFIED GTN MODEL"**, being submitted by **Mr. Praveen kumar Pathak,** in partial fulfillment of the requirement for the award of degree of **MASTER OF ENGINEERING (CAD/CAM & ROBOTICS) at THAPAR UNIVERSITY, PATIALA** is a bonafide work carried out by him under our guidance and supervision and no part of this thesis has been submitted for the award of any other degree.

Rahul chhibber

Mr. Rahul Chhibber
Lecturer
Mechanical Engineering Department.
Thapar University,
Patiala -147004

BK Dutta

Dr. Bijan Kumar Dutta
Head,
Computational Mech. Section
Reactor Safety Division
BARC
Mumbai-400085

9/1/2008

Dr S.K. Mohapatra
Professor & Head,
Thapar University,
Patiala -147004

RK Sharma

Dr R.K. Sharma
Dean, Academic Affairs
Thapar University
Patiala-147004

ACKNOWLEDGEMENT

A Thesis cannot be completed without the help of many people who contribute directly or indirectly through their constructive criticism in the evolution and preparation of this work. A special debt of gratitude is owed to my thesis supervisors, Mr. Rahul Chhibber (Lecturer, M.E.D) and co-supervisor Dr. B.K.Dutta (Head Computational Mechanics Section, BARC Mumbai) for his gracious efforts and keen pursuit which has remained as a valuable asset for the successful fulfillment of my Thesis. His dynamism and diligent enthusiasm have been highly instrumental in keeping my spirits high. His flawless & forthright suggestions blended with an innate intelligent application have crowned my task with success.

I would also like to offer my sincere thanks to Mr. Subashis Guin (SO-BARC Mumbai), all faculty, teaching and non-teaching, of Mechanical Engg. Deptt. (MED), and staff of central library, TU, Patiala for their assistance.

I am also thankful to the authors whose works I have consulted and quoted in this work. Last, but not the least, very special thanks to my parents and my friends for their constant encouragement and best wishes. Their patience and understanding without which this study would not have been in this present form, is greatly appreciated.

DATE: ***PRAVEEN KUMAR PATHAK***

(Roll No. 80681015)

ABSTRACT

Ductile fracture is associated with three basic processes i.e. void nucleation, growth and coalescence. The model which, incorporate these features into the constitutive equations of the material, are called continuum damage mechanics models. These are able to describe the physical effect of constraint on the fracture resistance of material in a natural way. In this work the model introduced by Gurson and modified by Tvergaard and Needleman has been implemented in an in-house finite element code MADAM. The material that is studied is SS 308L Weld filler and SS 309L Buttering. The two parameter approaches of fracture mechanics are discussed; also the J-R curve is determined for different cracked specimen, e.g. CT specimen, TPB specimens, from the analysis by finite element code MADAM and compared with the experimental curves. Also the various set of Gurson parameter is evaluated by comparison of experimental and analytical J-R curve to determine the fracture characteristics of nuclear welds.

CONTENTS

LIST OF FIGURES

LIST OF TABLES

NOMENCLATURE

SYMBOLS	STANDS FOR
a	Crack length
A_2	Constraint indexing parameter
a_i	Area of inclusion and void
b	Ligament length of specimen
B	Specific width, constant
CTOD	Crack tip opening displacement
D	Damage parameter/Diameter
ΔD	Contraction in diameter
E	Young's Modulus
E_t	Tangent modulus of stress- strain
f	Void volume fraction
f_o	Initial void volume fraction
f_c	Critical void volume fraction
f_f	Final void volume fraction
f_n	Void volume fraction at saturated nucleation
f	Void increment rate
f	Modified void volume fraction
f_u	Modified ultimate void volume fraction
f_{growth}	Void growth rate
$f_{nucleation}$	Void nucleation rate
G	Crack extention rate
G_c	Elastic energy release rate
J	J-integral
K	Acceleration factor
K_I	Stress intensity factor
K_{IC}	Plane stress fracture toughness
q	Multi-axiality quotient
q_1, q_2, q_3	Modifying parameters
Q	Triaxiality indexing parameter

R	Mean current void radius
R_0	Initial void radius
V_v	Volume fraction of voids
w	Specimen thickness
ε	Strain
ε_c	Strain corresponding to critical void growth ratio
σ_y	Yield stress

CHAPTER 1

INTRODUCTION

The nuclear weld between plain carbon steel components and stainless steel piping components are a necessity in pressurized water reactor (PWR) & pressurized heavy water reactor systems (PHWR).

The nuclear welds which are of interest are those attaching the piping systems to various nozzles of reactor pressure vessel, steam generators & pressurizes. These nuclear weld have zones with metallurgical discontinuities, the zones are immediately adjacent to each other and provide a variation of properties across a narrow region, this results in localization of strains. Further the geometrical discontinuity such as inclusion & fabrication defects, results in increasing the problem associated with life management and structural integrity assessment of these nuclear welds.

The local approaches provide methodology for fracture analysis of material taking into account the microstructure damage mechanics. The local approach to fracture is though to be able to deal with the problem of complex conditions and complex properties of the nuclear welds, as resulting from elaborate interaction of different microstructure with gradient in material properties.

The present work in this thesis uses the micromechanical modeling approach using modified GTN model to assess the fracture characteristics of these nuclear welds.

This thesis consists of seven chapters. The first chapter is the introduction to the thesis, provides a summery of the work carried out in the thesis and outlays the organization of the thesis into various chapters and their broad content.

Second chapter of the thesis is literature review related to various aspects of the current problem has been carried out and form the core of this chapter. It also review the state of art problem associated with nuclear welds, and discusses the structural integrity issue accompanying the nuclear welds & basics of damage mechanics models.

The third chapter of problem formulation identifies the present problems and defines it.

The fourth chapter deals with the experimental part and interpretation of the experimental work of the thesis. It provides the details of welding process and also provides the information regarding experimental determination of fracture characteristics of weld region of nuclear weld.

The fifth chapter is FE analysis methodology, describes the methodology adopted for finite element analysis being used in this work.

The sixth chapter is evaluation of gurson parameter, deals with the experimental determination of GTN model parameters & their analytical calibrations. It also deals with generation of J-R curves for CT and TPB specimens analytically & compares the experimental and analytical results for CT specimen to predict the fracture characteristics.

The seventh chapter summarizes the conclusion of present work and also provides the scope of future work in present area of investigation.

CHAPTER 2

LITERATURE REVIEW

2.1 Dissimilar welds in Nuclear Reactors [1]

Dissimilar welds are a challenge to fracture mechanics assessment procedures in determining the factors surrounding fracture and also impose an uphill task towards accurate materials characterization.

Several metallurgical design concepts can be used to make sound welds and the quantitative fracture mechanical properties can be related to different procedures. At present, the knowledge available regarding homogeneous weldments is being used for design, and no detailed methods exist for determining structural integrity of dissimilar welds.

Structural integrity assessment of dissimilar welds in its current form relies on practical methods derived on the basis of years of experience in operation and simplistic strength of materials analyses.

Complex conditions and properties of the weldment, as resulting from the interaction of different microstructures with gradients in material properties, have limited the ability of currently existing methods to construct the assessment on the basis of actual failure mechanisms of dissimilar welds.

Thus it can be emphasized that the high dissimilarity in properties are a hindrance to the assessment process, and effects of local micro- structures to the failure assessment still remain unanswered.

The area of concern in the structural integrity assessment of a weld is the micro-structural and mechanical heterogeneity of a weld.

It is seen that the variation of micro-structure across a weld leads to a variation of mechanical properties, such as toughness and stress-strain properties. Differences in

strain hardening capacities of micro- structural zones are found to severely affect the toughness transitions of the weld and the associated failure mode.

The effect of mismatch is to be considered for assessment when the variation in strength of mismatch materials exceeds 10 percent, starting from a few early publications e. g. **[2, 3]**; the bulk of the work in this area has been performed within the past decade**.** A large number of recent publications, e.g. **[4 – 9]**, and two international symposia **[10, 11]**, dedicated to the effects of yield strength mismatch on structural integrity, have shown the importance of mismatch problem..

There has been much interest in the analysis of mixed-mode fracture over many years. Direction of mixed-mode crack propagation model has been characterized by many direction criteria such as maximum tensile stress **[12]**, minimum strain energy density **[13]**, maximum tangent stress and maximum shear stress **[14]**, and maximum principle stress **[15]**.

These fracture criteria were combined with fracture criteria such as a stress intensity factor, CTOD or crack-tip opening angle (CTOA), and J-Integral. However, Finch **[16]** mentioned that none of these fracture criteria and direction criteria could represent the crack propagation behaviours. The combination of fracture criteria with the appropriate direction criteria is still under investigation. The combination of fracture criteria with the appropriate direction criteria is still under investigation.

2.2 Damage Mechanics [17]

2.2.1 Introduction

The fundamental difference between fracture mechanics and damage mechanics is that in damage mechanics we consider the void, nucleation and coalescence while in fracture mechanics we do not consider any voids formation in metal matrix. The distance between the nucleuses of two voids is of micro level that’s why it comes under micro mechanical Modelling.

In any engineering material, a number of microscopic voids are present initially in the metal matrix. These voids may be present due to the manufacturing process of the material itself or these may nucleate from the inclusions and second phase particles.

The ductile fracture (damage mechanics) is a process, which consist of nucleation, growth, and coalescence of these microscopic voids. The void coalescence leads to stable crack growth by merging of voids in the material. Void nucleation may arise from particle cracking. Void may also be formed by pipe-up of dislocations at highly disordered grain boundaries. In the first instance, the particle cracks and thereby separates itself from the matrix, leaving a void. In the later situation, the particle and the matrix separate at their interface without any cracking of the particle. Once formed, the voids grow under the applied loads also the growth rate depends on the size and shape of the voids & ligaments between the voids. Figure 2.1 show the Progress of fracture in a material due to damage

At some point, stresses in the ligament become high to the point where an unstable necking of the ligament takes place, this leads to the merging of two voids. The merging of two voids is known as the void coalescence or stable crack growth.

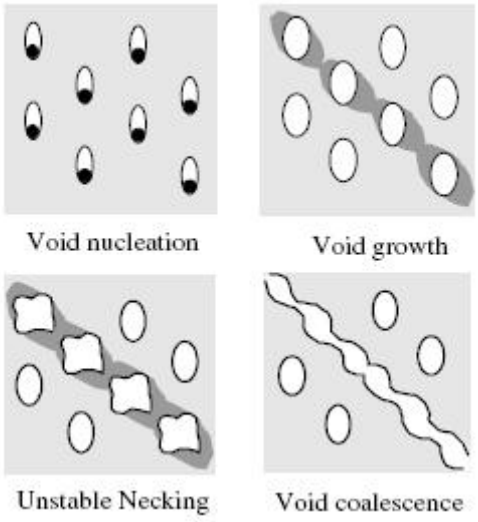

Figure 2.1 Progress of fracture in a material due to damage [17]

2.2.2 Local Approach in Fracture Mechanics (Damage Mechanics) [18]

2.2.2.1 Coupled type of models [18]

There exist several models of local approach, which are used to model ductile fracture. Some of the model incorporates a parameter called void volume fraction ‘f ‘into the constitutive relation ship of the material. This takes into account the softening effect due to the accumulation of the voids in the material. Here, a function, which describes the

process of nucleation, growth and coalescence of voids, is defined and is incorporated into the constitutive equation of the formulation. These types of models are called pours plasticity models or coupled type of models in local approach.

These are known as micro-mechanical models. Some of the models are Gurson-Tvergaard-Needleman's model and Rousellier-Seidenfuss models.

- **Gurson -Tvergaard –Needleman's Model for Ductile Fracture Simulation**

The model used in this study is based on a flow function introduced by Gurson and later modified by Tvergaard and Needleman. The micro-scopical ductile rupture process which is described by nucleation, growth, and coalescence of voids were introduced into the constitutive relationship by Gurson.

The continuum damage mechanics models, which are used to describe ductile fracture processes, are based on analysis of simple unit cell in which micro-void nucleation, growth and coalescence models are incorporated.

The void volume fraction 'f 'is defined as the ratio of the volume of voids to that of a unit cell. The increase in void volume fraction consists of two terms, i.e. void fraction increase due to nucleation of new void and due to growth of existing void. So

$$\dot{f} = \dot{f}_{nucleation} + \dot{f}_{growth} \tag{2.1}$$

The symbol (.) represents the increment of the quality. The expression for the increase in void fraction due to growth of void can derived from plastic incompressibility condition of the matrix material. It is given by

$$\dot{f}_{growth} = (1-f).\delta_{ij}.\dot{\eta}_{ij}^{P} \tag{2.2}$$

Where δ_{ij} is the kronecker delta function and η_{ij}^{p} is the plastic strain tensor. For calculating the void growth due to nucleation, an empirical relation was proposed by Needleman and Rice which is given as

$$\dot{f}_{nucleation} = A.\dot{\sigma}_{M} + \frac{B}{3}.\dot{\sigma}_{k}^{k} \tag{2.3}$$

Where σ_M is the actual flow stress of the matrix material and σ_k^k is the first stress invariant.

For stress controlled nucleation,

$$A = B = \left(\frac{1}{E_t} - \frac{1}{E} \right) \frac{f_N}{s_N \sigma_y \sqrt{2\pi}} \exp \left[-\frac{1}{2} \left(\frac{\sigma_M + \frac{1}{3}\sigma_k^k - \sigma_N}{s_N \sigma_y} \right)^2 \right] \qquad (2.4)$$

Where f_N is the volume fraction of void nucleation particle, σ_y is the yield stress of the matrix material and s_N is the slandered deviation of stress over which most of the voids nucleate. This model uses the in-house finite element code, MADAM, for analysis work to determine the J-R curves for the various specimens e.g. CT (compact tension) specimen, SENT (single edged notched tensile) specimen etc.

- **In-house damage Mechanics Code ,MADAM [18]**

As in-house finite element code MADAM (Material Damage Modelling) has been developed based on the principles of continuum damage mechanics (Modified Gurson's model).

Feature's of the code:

1. The code has the ability to solve both two and three dimensional structures. In 2D analysis, 4-noded and 8-noded isoperimetric elements are available. In 3D, 20 noded isoperimetric brick elements are available.
2. It can handle the 2- dimensional case of plain strain, plain stress and axi-symmetric structures under thermal-elastic-plastic deformations.
3. The geometric nonlinearity is considered by using the Lagrangian formulation.
4. The deformation and rotation in elastic-plastic analysis is considered by transforming the computed Cauchy stress to Jaumann stress rate using the corresponding spin rate tensor.
5. The frontal solution technique is used for solving linier set of simultaneous equations. The load-deformation equilibrium conditions are obtained by using Modified-Riks Algorithm.
6. For integration of elastic-plastic constitutive equations for the GTN yield model, the generalized mid-point algorithms formulate by Zhang has been used.
7. Both load and displacement controlled formulation.

- **Method of determination of Gurson parameter for the material [18]**

1. Initial void volume fraction 'f_0':- It represents the initial void fraction of the inclusions in the material which are not strongly adhered to the matrix. It is

determined by metallographic examination. But analysis of notched tensile test confirms the parameter.

2. Critical void volume fraction 'fc':- It is determined by numerical fitting of the point of drop of experimental load-deflection or load-diametral contraction curve of the notched tensile specimen.

3. Void volume fraction at saturated nucleation 'f_n':- It is determined by metallographic examination as well as fitting of numerical analysis data with experimental data.

4. Final void volume fraction at fracture 'f_f':- It is determined by metallographic examination.

5. Mean strain of void nucleation 'ϵ_n':- It is determined by conducting tensile test and subsequent metallographic examination.

6. Standard deviation of nucleation strain 'S_N':- The value of Standard deviation of nucleation strain is assumed generally as 0.1 for steel. It does not have much effect on the results of analysis. It represents the scatter of nucleation strain. It can be determined from metallographic study of nucleation process of voids and finding the statistical distribution.

7. q_1 = 1.5, q_2 = 1.0, q_3 = 2.25:- These values are usually not changed. But some studies suggest that these parameters are also material dependent.
8. Critical length parameter 'l_c':- It represents the mean spacing of inclusion which is responsible for void nucleation. For cracked specimens, it represents the mean distance of a potential inclusion ahead of crack tip. It is determined by analysis of cracked specimens and comparison of J value with the experimental value.

2.2.2.2 Uncoupled type of models [18]

In this case, the damage variable does not affect the constitutive behavior of the material. The damage and material flow (yielding) behavior are uncoupled. The material is assumed to follow the von-mises yield criteria with either isotropic hardening. A damage

variable is defined which is a function of local stress and strain in the matrix material. The local stresses and strains are computed from conventional elastic-plastic finite element analysis. The damage variable is computed at each gauss point in the finite element mesh of the structure with respect to increased applied loading. The critical value of this parameter is determined before hand from simple tension tests. When the critical value of the parameter is reached, the ductile fracture is assumed to initiate in the structure. These types of the models are called continuum mechanics models or locally uncoupled type of models.

Some of these models are: Rice and Tracey's cavity growth model, Budiansky and Coll.'s model, Tai and Yang's model etc.

- **Rice and Tracey's model**

It is the most popular method which is used in the local approach for modeling ductile fracture process. It gives a critical parameter, which corresponds to the process of void coalescence in the material. The critical parameter can not be used as a true material property to predict crack initiation in a component of the material. So a modified Rice and Tracey's model has been proposed in the form of two additional parameters, i.e. q_1 and q_2. In Rice and Tracey's model the damage parameter is considered to be the equivalent cavity radius 'R'. The growth of an isolated void in an infinite block of an elastic and plastic stain hardening material is given by the expression:

$$\frac{\delta R}{R} = \alpha \delta \varepsilon_{eq}^{p} \exp\left(\frac{3\sigma_m}{2\sigma_{eq}}\right)$$, where is constant factor. For high stress triaxialities, $\alpha = 0.283$.

2.3 Review of Work

As the historical back ground of the subject, one of the earlier references by gurson in 1977 is printed indicating the determination of damage characteristics of the cracks, occur within the different materials. Further, different authors and scientists give various approaches relating to the damage and fracture behavior of the material.

S. Dhar et al [19] discuss about a continuum damage mechanics model for ductile fracture. Continuum damage mechanics theory together with large deformation elastic–

plastic finite element analysis has been used to predict crack growth initiation in ductile materials. The damage growth law is based on experimental observations reported in the literature. A local crack growth initiation criterion is proposed. The criterion makes use of the critical damage as the continuum parameter and the average austenite grain size as the characteristic length. To test the validity of this criterion, experiments have been conducted on standard specimens and have also been simulated numerically. The proposed criterion has been used to predict the values of the critical load at crack growth initiation and the fracture toughness. The numerically predicted values compare favorably with the experimental values.

E. Schnack and W. Weikl [20] give the Shape optimization under fatigue using continuum damage mechanics. An introduction and overview of the developments in shape optimization for fatigue problems is given, beginning with the main ideas in the field of static shape optimization. The use of numerical tools together with the incorporation of non-linear material properties in the continuum mechanics design has led to new possibilities for the analysis of fatigue behaviour in mechanical engineering structures. Based on publications by Lemaitre and Chaboche, the material behaviour is described by defining different partial differential equation systems on micro-scale and meso-scale. From this an optimal algorithm results for the shape optimization of mechanical engineering structures using continuum damage mechanics. Our numerical and experimental tests show a significant increase of lifetime in comparison to classical shapes.

S. Tarafder et al [21] discuss about the ductile fracture behaviour of primary heat transport piping material of nuclear reactors. Design of primary heat transport (PHT) piping of pressurised heavy water reactors (PHWR) has to ensure implementation of leak-before-break concepts. In order to be able to do so, the ductile fracture characteristics of PHT piping material have to be quantified. In this paper, the fracture resistance of SA333, Grade 6 steel – the material used for Indian PHWR – under monotonic and cyclic tearing loading has been documented. An attempt has also been made to understand the mechanism responsible for the high fracture toughness of the steel through determination of the effect of constraint on the fracture behaviour and fractographic observations. From J –R tests over a range of temperatures; it was observed that SA333 steel exhibits embrittlement tendencies in the service temperature regime.

The fracture resistance of the steel is inferior in the longitudinal direction with respect to the pipe geometry as compared to that in the circumferential direction. Imposition of cyclic unloading during ductile fracture tests for simulation of response to seismic activities results in a dramatic decrease of fracture resistance. It appears, from the observations of effects of constraint on fracture toughness and fractographic examinations, that fracture resistance of the steel is derived partly from the inability of voids to initiate and grow due to a loss of constraint in the crack-tip stress field.

J. Chattopadhyay et al [22] gives a discussion on Fracture experiments on through wall cracked elbows under in-plane bending moment: Test results and theoretical/numerical analyses. Fracture assessment of pipe bends or elbows with postulated through wall crack is very essential for leak-before break qualification of primary heat transport system piping of nuclear power plants. The methodology for fracture assessment of cracked elbows is still in developing stage. Any new development in theoretical aspect requires experimental validation. However, fracture test data on cracked elbows is not as abundant as straight pipes. The earlier experiments on cracked elbows were focused mainly on the determination of limit load. Other fracture parameters e.g. crack growth, crack initiation load or crack opening displacement was not reported in the open literature. Against this backdrop, a comprehensive experimental and theoretical program on component integrity has been initiated at Reactor Safety Division (RSD) of Bhabha Atomic Research Center (BARC), India. Under this program, a number of fracture tests have been carried out on elbows with through wall circumferential/axial cracks subjected to in-plane closing/opening bending moment. These test data are then thoroughly analyzed numerically through non-linear finite element analyses, analytically through limit load comparison and also through comparison of crack initiation loads by finite element and R6 methods. These test data may be utilized in future for validation of new theoretical developments in the integrity assessment of through wall cracked elbows.

Xiaosheng Gao et al [23] focused on the ductile fracture initiation toughness: Effects of void volume fraction void shape and void distribution. This paper studies the effects of the initial relative void spacing, void pattern, void shape and void volume fraction on ductile fracture toughness using three-dimensional, small scale yielding models, where voids are assumed to pre-exist in the material and are explicitly modeled using refined finite elements. Results of this study can be used to explain the observed fracture

toughness anisotropy in industrial alloys. The analyses suggest that simplified models containing a single row of voids ahead of the crack tip is sufficient when the initial void volume fraction remains small. When the initial void volume fraction becomes large, these simplified models can predict the fracture initiation toughness (J_{Ic}) with adequate accuracy but cannot predict the correct J–R curve because they over-predict the interaction among growing voids on the plane of crack propagation. Consequently, finite element models containing multiple rows of voids should be used when the material has large initial void volume fraction.

V. Tvergaard et al [24] presents the three dimensional micro-structural effects on plane strain ductile crack growth. Ductile crack growth under mode I, plane strain, and small scale yielding conditions is analyzed. Overall plane strain loading is prescribed, but a full 3D analysis is carried out to model three dimensional micro-structural effects. An elastic-viscoplastic constitutive relation for a porous plastic solid is used to model the material. Two populations of second-phase particles are represented, large inclusions with low strength, which result in large voids near the crack tip at an early stage, and small second-phase particles, which require large strains before cavities nucleate. The larger inclusions are represented discretely and the effects of different three dimensional distributions on the crack path and on the overall crack growth rate are analyzed. For comparison purposes, a two dimensional distribution of cylindrical inclusions is analyzed. Crack growth occurs off the initial crack plane in all 3D computations, whereas straight ahead crack growth occurs with the two dimensional cylindrical inclusions. As a consequence, the three dimensional distributions of spherical inclusions exhibit an increased crack growth resistance as compared to the two dimensional distribution of cylindrical inclusions.

M. Mashayekhi et al [25] found the ductile crack growth based on damage criterion: Experimental and numerical studies. The continuum mechanical simulation of the micro-structural damage process is important in the study of ductile fracture mechanics. In this paper, the continuum damage mechanics framework for ductile materials developed by Lemaitre has been validated experimentally and numerically for A533-B1 alloy steel under triaxial stress conditions. An experimental procedure to identify the damage parameters was established and the experimental calibrated damage parameters were then used in a finite element model. A fully coupled constitutive elastic–plastic-damage model

has been developed and implemented inside the ABAQUS implicit FEA code. The model is based on a simplified Lemaitre ductile damage model whose return mapping stage requires the solution of only one scalar non-linear equation. A local crack growth criterion based on the critical damage parameter was proposed; the validity of this criterion was examined by comparing the simulation with the experimental results on standard three point bending (3PB) test. The critical load at crack growth initiation and the fracture toughness, J_{Ic}, has also been predicted from the simulation. These numerically predicted values compared favorably with those obtained from experiments.

A. Abou-Chakra Guéry et al [26] presented about the micromechanical model of elastoplastic and damage behavior of a cohesive geomaterial. The present study is devoted to the development and validation of a nonlinear homogenization approach of the mechanical behavior of Callovo-Oxfordian materials. The material is modeled as a heterogeneous composite composed of an elastoplastic clay matrix and of linear elastic or elastic damage inclusions. The macroscopic constitutive law is obtained by adapting the incremental method proposed by Hill. The approach consists in formulating the macroscopic tangent operator of the material by considering the nonlinear local behavior of each phase. Due to the matrix/inclusion morphology of the microstructure of the materials, a Mori–Tanaka scheme is considered for the localization step. The developed model is first compared to Finite Element calculations and then validated and applied for the prediction of the macroscopic stress–strain responses of materials.

T V Pawan Kumar, J Chattopadhyay, B K Dutta & H.S Kushwaha [27] the mechanical integrity of PHWR components based on fracture mechanics requires the determination of J-R curves obtained from specimens. These J-R curves are geometry dependent and the transferability of specimen J-R curves to component level is questionable. The influence of crack tip constraint or stress triaxiality has been emphasized recently in explaining the geometry dependent resistance of specimens and structures to ductile tearing. The Q and h are used as crack tip constraint indexing parameters. Two dimensional plane strain elastic plastic analysis have been carried out on three point bend bar (TPBB) and compact tension (CT) specimen to study the characteristics of Q and h parameters. It is observed that h is dependent on both distance and angular position. Hence the third parameter is required where h value has to be evaluated to consider it for local fracture criterion. It is identified that Q can be used as

constraint indexing parameter along with the J- integral to characterise the crack tip stress state. For high constraint geometries this relationship is not valid at high deformation level.

CHAPTER 3

PROBLEM FORMULATION

Some of the major problems the structural engineers have to cope with in fracture analysis are material characterization (i.e. generation of adequate data from specimen testing) and transferring of fracture mechanics material data to the structural analysis of components. As a matter of fact, the generation of material data is expensive and time consuming. For example, the determination of J-resistance curve is still a cumbersome task. Also the existing material data often do not correspond to the specific application (i.e. in reference to temperature, strain rate, irradiation etc.) and hence extrapolations are necessary, which may not represent the actual behavior. Hence the transferring of fracture mechanics data to real life components may be questionable, especially if complex situations are involved including heterogeneous materials, residual stresses, thermo mechanical loading, historical effects, and different state of stress triaxiality at the crack tip, constraint effects and many other factors.

In work of continuum mechanics, Gurson first derived the yield potential for porous material with voids and introduced the model for analysis of ductile fracture which was later modified by Tvergaard and Needleman. If one uses this model, he can simulate the crack initiation and growth as this happens in the material without resorting to artificial numerical technique. So, the effect of stress multiaxiality on the fracture resistance behavior is automatically taken care of and one can predict fracture behavior of any component with any geometry and loading conditions.

In House Damage Code MADAM (Material Damage Modeling) provided by BARC, based on GTN model, is used to determine fracture characteristics of SS308L and SS309 welded specimen.

CHAPTER 4
EXPERIMENTATION

4.1 Introduction

The Gurson parameters were determined by curve fitting of experimental and analytical results. The curve fitting is generally done using load-ΔD curves of round notched tensile specimens of R2 (Notch radius 2mm) & R4 (Notch radius 4mm). In curve fitting the Gurson parameters are varied so that the analytical curve approximates the experimental one in terms of load dropping point and slope of curve at sudden load drop. The experiments were performed at BARC & at IIT ROORKEE and data was provided. This chapter describes the results of tests conducted for damage mechanics analysis.

4.2 Material Properties and Composition

4.2.1 Material properties for SS 308L Weld filler

Weld filler SS 308L has the same composition as type SS 308 except the carbon content has been held to a maximum of .03% to reduce the possibility of intergranular carbide precipitation.

This is ideal for welding Types 304L, 321 and 347 stainless steels. This is a suitable wire for applications at cryogenic temperatures.

Category	Steel
Class	Stainless steel
Type	Austenitic nonstandard
Common Names	Chromium-Nickel steel

Table 4.1 Description of SS 308L weld

Chemical composition:

Elements	% Composition
Carbon	0.030
Manganese	1.000-2.500
Silicon	0.300-0.650
Chromium	19.500-21.000
Nickel	9.000-11.000
Molybdenum	0.300
Sulfur	0.020
Phosphorus	0.030
Copper	0. 300

Table 4.2 Chemical compositions of SS 308L

Mechanical Properties:

Density (×1000 kg/m^3)	7.7-8.03
Poisson's Ratio	0.27-0.30
Elastic Modulus (GPa)	190-210
Tensile Strength (MPa)	618
Yield Strength (MPa)	448-460

Table 4.3 Mechanical properties of SS 308L

4.2.2 Material properties for SS 309L Buttering filler

SS 309L is a highly alloyed austenitic stainless steel used for its excellent oxidation resistance, high temperature strength and creep resistance. The lower nickel content of SS 309L improves resistance to sulphur attack at high temperatures. It is tough and ductile, and can be readily fabricated and machined.

Chemical Composition:

Component	C	Cr	Fe	Mn	Ni	P	S	Si
Wt. %	0.2	22-24	57-62	2	12-15	0.045	0.03	0.75

Table 4.4 Chemical composition of SS 309L

Mechanical Properties:

Density (×1000 kg/m^3)	7.7-8.03
Poisson's Ratio	0.27-0.30
Elastic Modulus (GPa)	190-210
Tensile Strength (MPa)	644
Yield Strength (MPa)	489

Table 4.5 Mechanical properties of SS 309L

4.2.3 Material properties for German steel (20MnMoNi55)

The one of the specimen plate used in this work is German steel, the Mechanical and Chemical properties are given in table 4.6 & table 4.7 respectively**.**

Material Properties	Value
Young's Modulus	2.05 x 10^5 MPa
Ultimate Tensile Strength	627.6575 MPa
Yield strength	552.4323 MPa
Poisson's Ratio	0.29
% Elongation	22%

Table 4.6 Mechanical properties of 20MnMoNi55 steel

Chemical Composition of 20MnMoNi55													
Components	C	Si	Mn	P	S	Cr	Ni	Mo	N	Cu	Al	Sn	As
[Wt-%]	0.21	0.24	1.48	0.008	0.005	0.2	0.8	0.52	0.02	0.07	0.015	0.005	0.02

Table 4.7 Chemical composition of 20MnMoNi55 steel

4.2.4 Material properties for Stainless steel (SS 304)

Chemical composition:

Components	C	Si	Mn	P	S	Cr	Ni	N
Wt %	0.08	0.75	2.0	0.045	0.030	20.0	10.5	0.10

Table 4.8 Chemical composition of SS 304

Mechanical properties:

Material Properties	Value
Young's Modulus	193 GPa
Ultimate Tensile Strength	515 MPa
Yield strength	205 MPa
Poisson's Ratio	0.29
% Elongation	22%

Table 4.9 Mechanical properties of SS 304

4.3 Engineering stress-strain curves for SS 308L

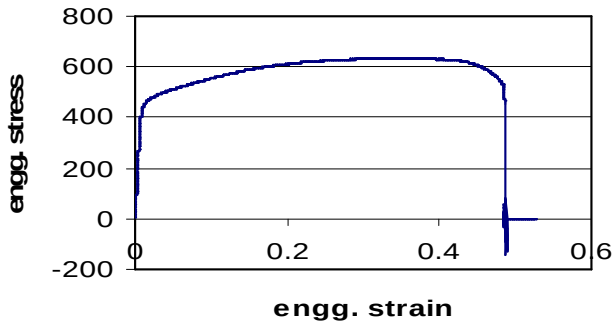

Fig 4.1 Engineering Stress-Strain curve for SS 308L

4.4 Engineering stress-strain curves for SS 309L

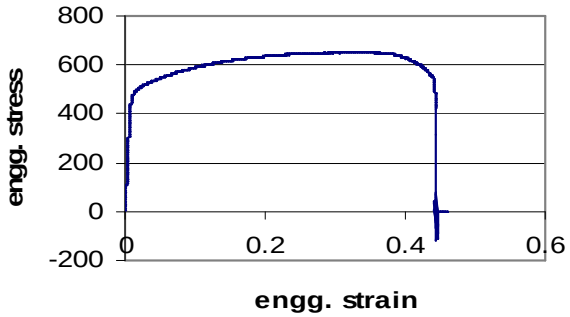

Fig 4.2 Engineering stress-strain curve of SS 309L

Now using these engineering stress-strain curves, draw the true stress-strain curve and then using the linear curve fitting technique, extrapolate the curve and take the stress-strain data within the plastic region, above the yield point.

4.5 Experimental load – ΔD (Diametrical Contraction) curves of Round Notched Tensile specimens

Tensile test results of RNTS were taken from RSD, BARC. Results were given in the form of time vs load and material diametric contraction was recorded using digital camera which takes 25 images per second. These images were processed to find diametric contraction of round notch tensile specimen.

4.5.1 Details of the Round Notched Tensile Specimens

There are two notched tensile specimens with notch groove radius 2mm and 4mm, designated as RNTS R2 and RNTS R4. The geometry of specimens is shown in Figure 4.3.

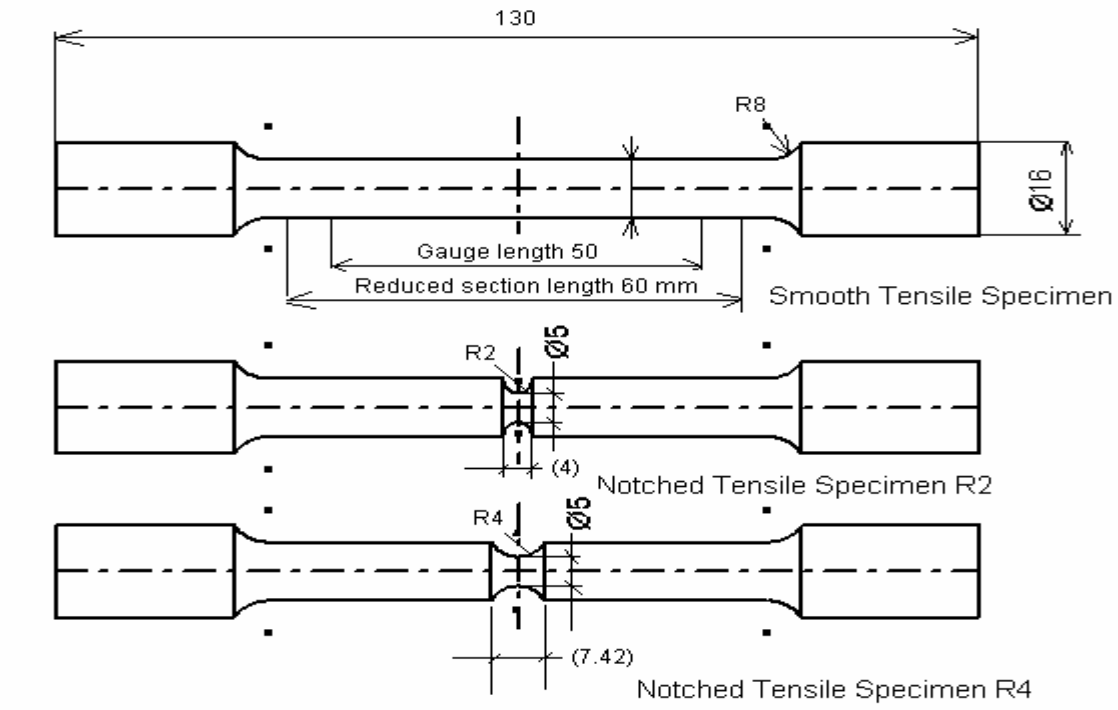

Fig 4.3 Detail of smooth and notched tensile specimens

The results of tests were recorded in the form of images (Fig 4.4) and instantaneous load values from the digital display. The images were then post-processed with Photoshop software. The images were copied and pasted in Photoshop. Then the round piece diameter and notch diameter were measured. The notch diameter was calculated by taking the reference diameter of cylindrical part as 10mm.

Let Measured notch diameter =d

Cylindrical part diameter =D

Now as we know that the diameter of cylindrical part is 10mm

So we can find out notch diameter as:

Notch diameter = (d/D) x 10 mm

Diametric contraction (ΔD) = Initial Notch diameter –Notch diameter

Initial notch diameter is 5mm.

Fig 4.4 Photographs during testing of SS 308L R2

4.5.2 Test results for RNTS

The Load vs ΔD (diametrical contraction) is plotted from the result obtained from the image processing for both R2 and R4. The plot of load vs. ΔD for SS 308L R2 and SS 308L R4 is shown in figure 4.5 and figure 4.6 respectively.

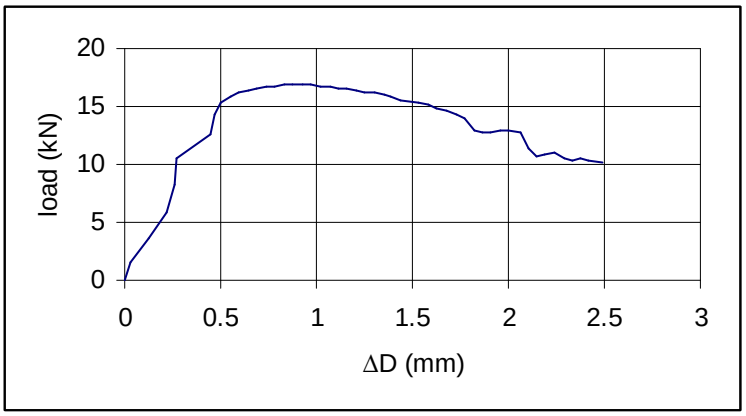

Fig. 4.5 Experimental Load-ΔD curve for R2

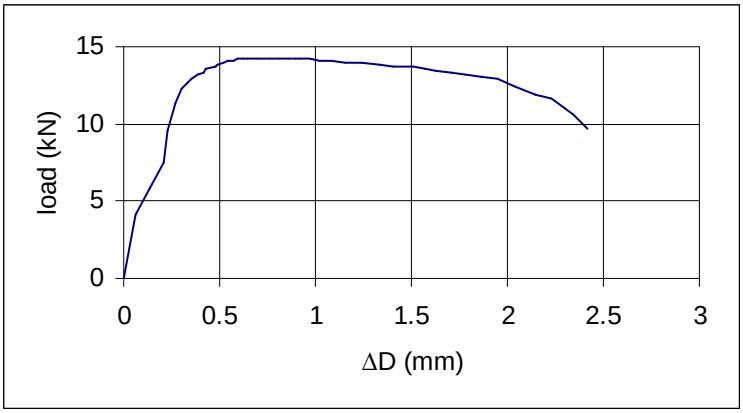

Fig 4.6 Experimental Load-ΔD curve for R4

Similarly the experimental load vs. ΔD curve for SS 309L buttering for notch radius 2mm and 4mm can be drawn. Some photograph of SS 309L R4 is shown in figure 4.7.Due to not having sufficient data and photograph for notch radius 2mm (R2), the experimental curve for radius 2mm is not shown, here the experimental curve for notch radius 4mm (R4) of SS 309L is shown in figure 4.8.

Fig 4.7 Photographs during testing of SS 309L R4

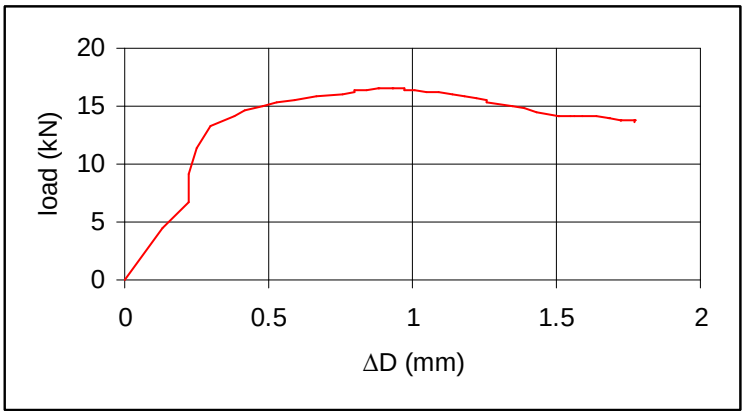

Fig 4.8 Experimental Load-ΔD curve for R4

4.6 Welding and Specimen Preparation for CT and TPB Specimens

The first stage of preparation of Specimen for testing is shaping of plates, one of them is German steel (20MnMoNi55) and other is stainless steel (SS 304), so that they become a weld coupon. The stainless steel plates is shaped using shaper and a slope of about 22.5 degree with the vertical is made such that when both the plates kept in front of each other for welding, a single-J is formed through out the length.

Now in second stage of preparation a buttering layer is deposited, as shown in figure 4.11, up to 6mm with SS 309L over welded side of mild steel work piece to avoid common welding defects.

Third stage of preparation is keeping these two plates in front of each other with 2 mm gap such that a single-j is formed through out the length and these plates are held by a backing plate (Mild Steel) along the length. Now the groove is filled by the spool or wire of either SS 308L or SS 309L as the case may be, using the TIG welding. The current during the welding is recorded around 200-225 ampere and arc voltage around 20-25 volt. The time taken to fill one complete coupon is around 6-8 hours. The welded work piece is then slowly cooled and backing plate is removed using grinder. Now the welded work piece is machined properly and cut by the machine to prepare the CT and TPB specimen of required dimension for testing of fracture characteristics. The different stages of preparation are shown in figure 4.9 to 4.14.

Welding Parameters used for TIG welding

Welding current:	200-225 ampere
Arc Voltage:	20-25 volts
Direct Current:	Electrode –Ve,
Shielding Gas:	99.99 % Argon,
Gas Flow rate:	10 to 20 CFH.

Fig 4.9 TIG welding machine

Fig 4.10 Complete setup for welding

Fig 4.11 Buttering layer over Mild Steel

Fig 4.12 Two welded plate with backing plate

Fig 4.13 Welded plates of SS 308L without backing plate

Fig 4.14 Welded plates of SS 309L

4.7 Testing of CT Specimen

The dimensions of CT specimen are given in fig 4.15 and the details of the testing procedure are discussed below.

4.7.1 Details of the Test Specimens

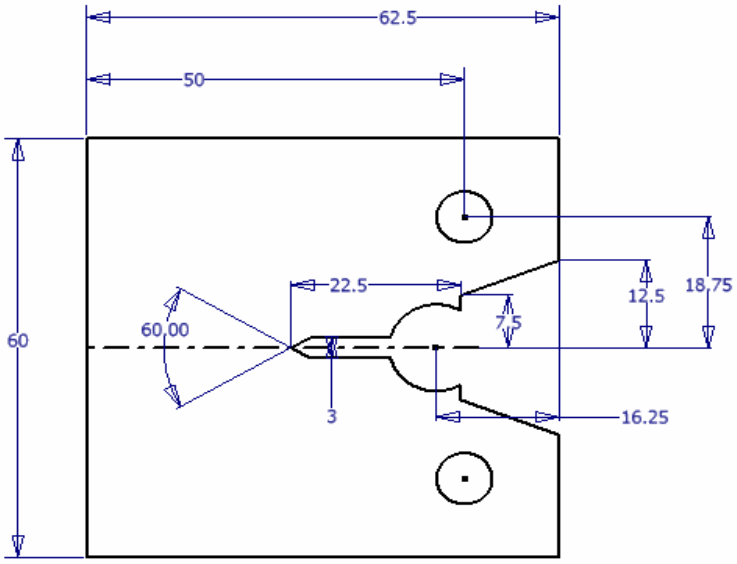

Fig 4.15 Details of the CT specimens

4.7.2 Details of the Testing Procedure

The specimens were pre-cracked (2-2.5mm) by cyclic loading. Crack opening displacement was measured using displacement gauge attached to the knife edge. Crack growth was calculated by monitoring the specimen compliance at each instant of unloading and employing a relation. The load, load-line displacement and crack-growth were processed to obtain the J-integral vs. crack growth. Pre-crack load was calculated as below. Only the maximum load is different for SS 308L & SS 309L, while $f(a_i/W)$ is same for SS 308L & SS 309L.

1. Pre-crack load for SS 308L

For CT Specimen

All specimens shall be precracked in fatigue at a force value based upon the Maximum force, Pm as follows:

$$\text{Maximum load} \quad Pm=\frac{0.4Bb_o^2\sigma_y}{(2W+a_i)} \quad =33.6 \text{ kN} \tag{4.1}$$

$$f(\frac{a_i}{W})=\frac{[(2+\frac{a_i}{W})(0.886+4.64(\frac{a_i}{W}) \ -13.32(\frac{a_i}{W})^2+14.72(\frac{a_i}{W})^3-5.6(\frac{a_i}{W})^4)]}{(1-\frac{a_i}{W})^{3/2}} = 8.34 \tag{4.2}$$

Where,

Specimen Thickness B= 25mm

Width of specimen W =50mm

Crack length a_i =22.5mm

Remaining width b_o =27.5mm

Yield strength σ_{ys} =448 Mpa

Ultimate Tensile Strength σ_{uts} =618 Mpa

Average yield strength $\sigma_y = (\sigma_{ys}+ \sigma_{uts})/2$ = 533 Mpa

For TPB Specimen

$$Pm=\frac{0.5Bb_o^2\sigma_y}{S} \quad = 24.72 \text{ kN} \tag{4.3}$$

$$f(\frac{a_i}{W}) = \frac{3(\frac{a_i}{W})^{1/2}[1.99 - (\frac{a_i}{W})\ (1-\frac{a_i}{W})(2.15 - 3.93(\frac{a_i}{W}) + 2.7(\frac{a_i}{W})^2)]}{2(1+2\frac{a_i}{W})(1-\frac{a_i}{W})^{3/2}} = 3.08 \quad (4.4)$$

Where,

Specimen Thickness B= 25mm

Width of specimen W =50mm

Crack length a_i =22.5mm

Support span S= 200mm

Remaining width b_o =27.5mm

Yield strength σ_{ys} =448 Mpa

Ultimate Tensile Strength σ_{uts} =618 Mpa

Average yield strength $\sigma_y = (\sigma_{ys} + \sigma_{uts})/2$ = 533 Mpa

2. Pre-crack load for SS 309L

For CT specimen

Average yield strength $\sigma_y = (\sigma_{ys} + \sigma_{uts})/2 = (489+644)/2$= 566.5 Mpa

Maximum load $Pm = \frac{0.4Bb_o^2\sigma_y}{(2W+a_i)}$ =34.97 kN

For TPB specimen

Average yield strength $\sigma_y = (\sigma_{ys} + \sigma_{uts})/2$ = 566.5 Mpa

Maximum load $Pm = \frac{0.5Bb_o^2\sigma_y}{S}$ = 26.78 kN

4.7.3 Experimental results for CT specimen

The CT specimens of ASTM standard were tested at IIT Roorkee. The experimental J-R curve is plotted from the data obtained after testing the CT specimen of SS 308L and SS 309L.

1. **Experimental J-R curve for SS 308L weld CT specimen**

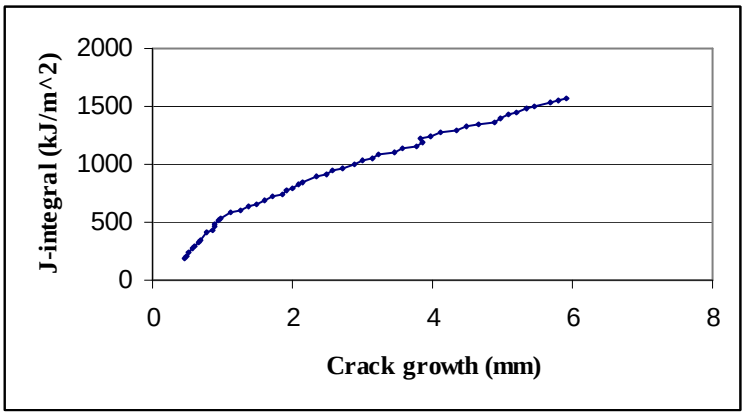

Fig 4.16 Experimental J-R curve for SS 308L weld CT specimen

2. Experimental J-R curve for SS 309L buttering CT specimen

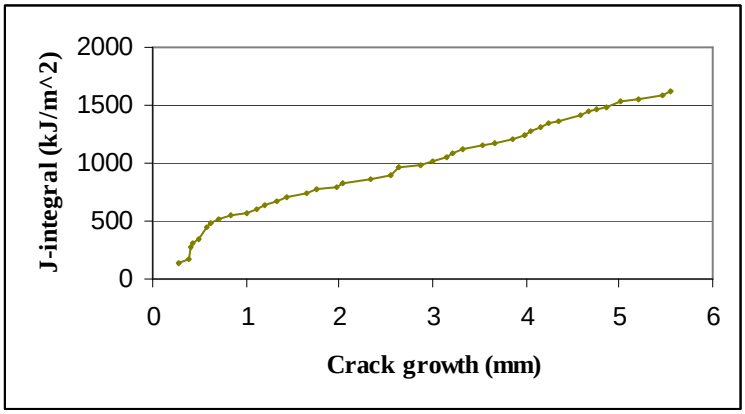

Fig 4.17 Experimental J-R curve for SS 309L buttering CT specimen

CHAPTER 5

ANALYSIS METHODOLOGY

5.1 Introduction

Analysis is divided into four steps

I. Generation of FE 2D- mesh
II. Input file preparation
III. Running the MADAM Code (Material Damage Modeling)
IV. Post-processing the output from code

5.2 Generation of FE 2D- mesh

The meshes for Notched Tensile Specimen, CT and TPB were generated using in house code FEMSHAPE. In case of RNTS as the specimen has two axis of symmetry, only one fourth of the specimen was modeled and in case of CT and TPB specimens have one axis of symmetry , only one half of the specimen was modeled. The geometric models were made such a way that the mesh size near the crack tip was equal to two times the critical length. Meshes away from the crack path were intentionally made large to reduce computational time. All the elements were 2D 8-node iso-parametric elements. The output file of fem shape was used to make input file for MADAM code. 2D mesh generated for RNTS R2 (2mm radius) and R4 (4mm radius) is shown in figure 5.2 and 5.3 respectively.

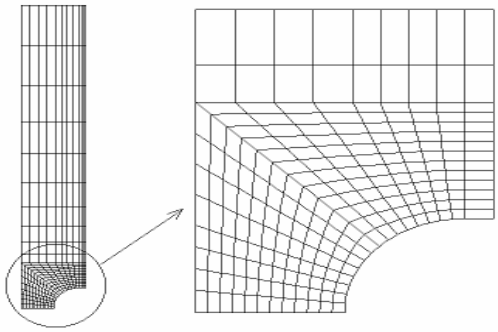

Fig 5.1 Mesh for RNTS R2 specimen

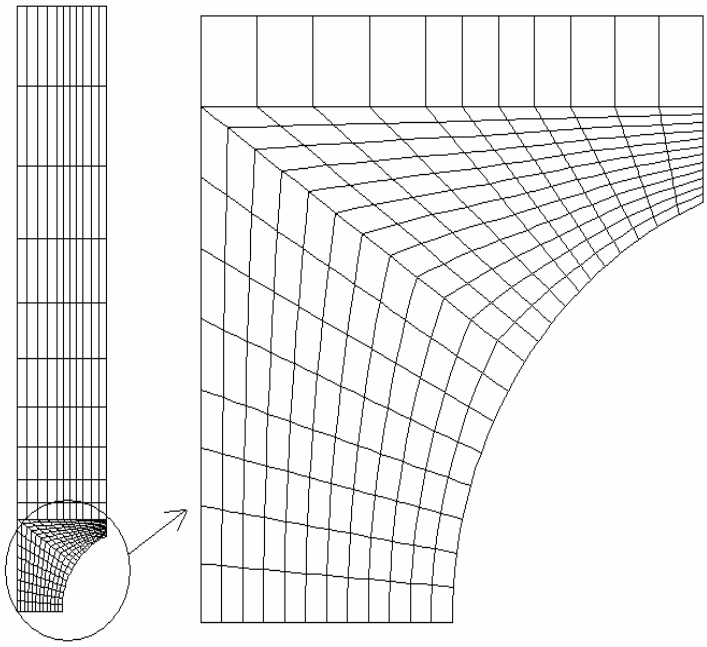

Fig 5.2 Mesh for RNTS R4 specimen

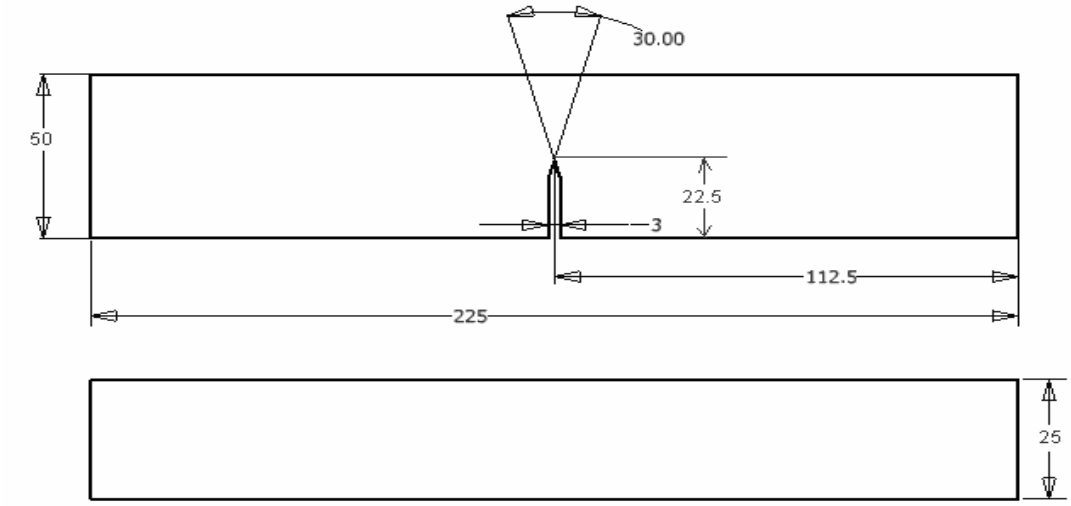

Fig 5.3 Geometry of TPB specimen

In case of TPB and CT as the specimen has one axis of symmetry, so only one half of these specimens are modeled. Geometry of TPB and CT specimens are given in Figure 5.4 & 5.6 respectively and corresponding FE meshes are given in Figure 5.5 & 5.7 respectively.

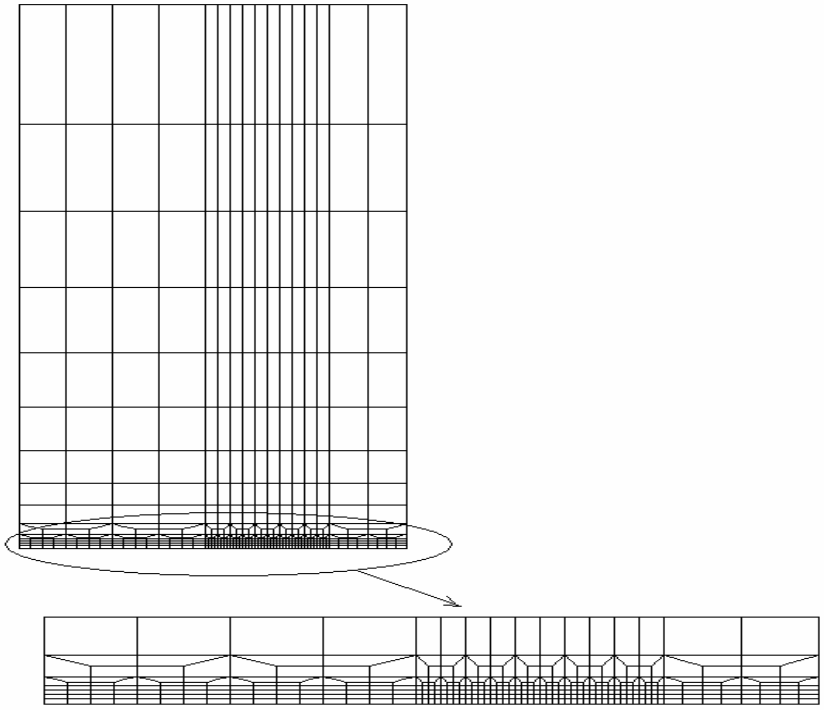

Fig 5.4 FE mesh for TPB specimen

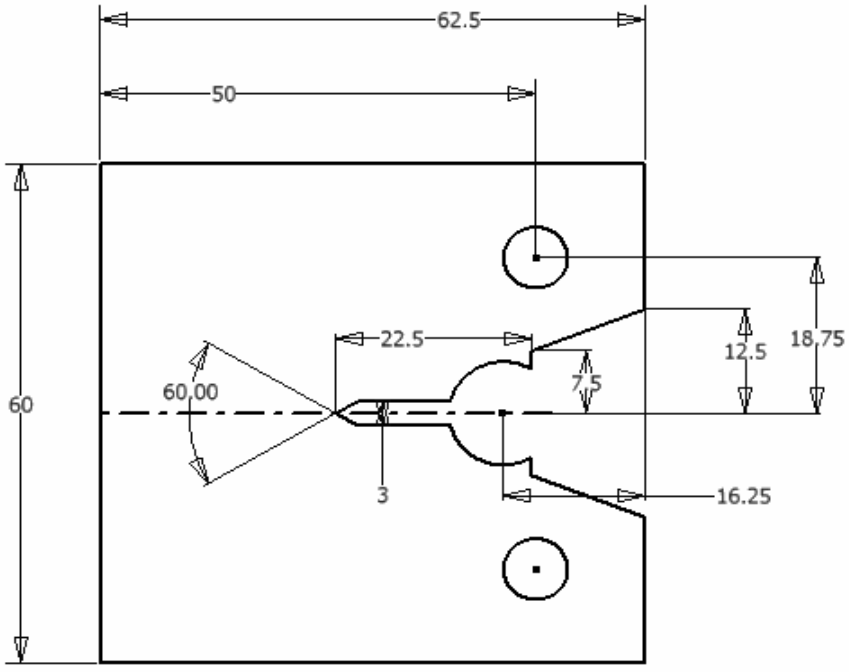

Fig 5.5 Geometry of CT specimen

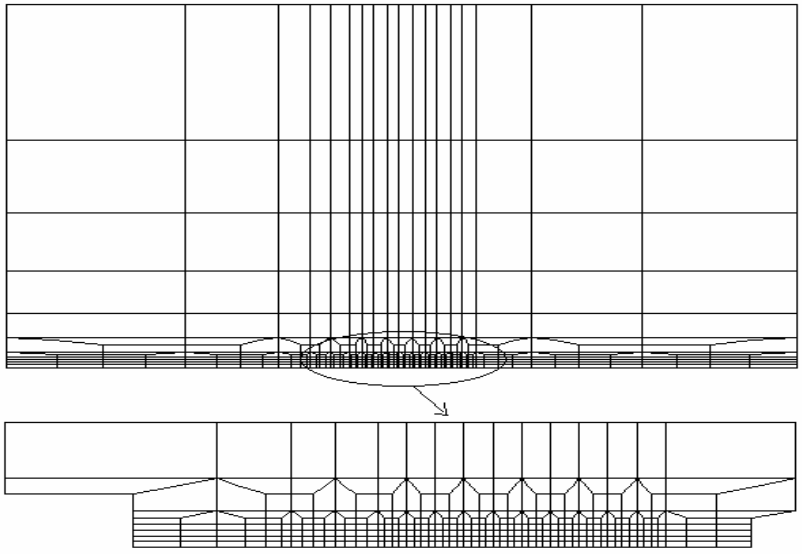

Fig 5.6 FE mesh for CT specimen

5.3 Input file preparation

Once the mesh has been constructed the next step is to prepare the input file for the component giving every detail that describes actual problem under investigation. The input file is then used by MADAM code. The input file is written in the following format

Card 1

First word (A10): Name of equation solver- SPRASE, FRONTAL, COLSOL (column solver), LPCG (linear pre-conditioned conjugate gradient solver).

Second word (A10): Solution technique- NEWTON (Newton-Raphson method), RIKS (Modified Rik's method).

Third word (A10): Integration scheme employed- MIDPOINT, BEULER (backward Euler), FEULER (forward Euler).

Card 2

This card set (A80) describes title to the problem.

Card 3

First data (I5): Total number of elements

Second data (I5): Total number of nodes

Third data (I5): Total number of nodes per element

Fourth data (I5): Number of elements for which the node relations are to be provided

Fifth data (I5): Number of nodes for which the coordinates are to be provided

Sixth data (I5): Index for loading condition -1 (Plane stress), 2 (plane strain), 3 (axis-symmetric case), 4 (3-D case).

Card 4

First data (I5): Number of materials

Second data (I5): Type of stress strain curve- 1 (true stress- true strain), 2 (engineering stress engineering strain)

Third data (I5): Type of analysis-0 (elastic –plastic), 12 (damage mechanics)

Fourth data (I5): Index for material hardening-0, (isotropic hardening), 1 (kinematics hardening)

Card 5

First data (I5): Number of group of boundary conditions

Second data (I5): Total number of boundary nodes

Third data (I5): Number of group of loads

Card 6

First data (I5): Index for geometric non-linearity-1(On), 0(Off)

Second data (I5): Number of load increments

Third data (I5): Maximum number of iteration for convergence

Fourth data (I5): Number of group of load fractions

Fifth data (I5): Number of print interval for output files.

Card 7

Here element and node relationship is provided which has been obtained through the mesh generating code or software.

For 2D 4-node iso- parametric quadrilateral element

First data (I5): Elements ID

Second data (I5): Material ID

Third to sixth data (I5): ID of corner nodes

For 2D 8-node iso- parametric quadrilateral element

First data (I5): Elements ID

Second data (I5): Material ID

Third to sixth data (I5): ID of corner nodes (anticlockwise)

Seventh to tenth data (I5): ID of corresponding mid - nodes (anticlockwise)

Card 8

Here the co-ordinates in x, y and z direction for each node are provided as obtained through the mesh generating code or software.

Card 9

Depending upon the number of groups of boundary conditions data are to be provided in this card.

Card 10

In this card material properties are given.

First data (E10.3): young's modulus of elasticity in MPa of material

Second data (E10.3): Poisons ratio

Third data (E10.3): Yield stress

Fourth data (I5): Number of data points for stress strain curve

Card 11

This card gives the data for stress-strain curve and immediately follows the card where young's modulus is provided.

Card 12

This card is only to be read when the 3^{rd} data in 4^{th} card is 1. The data are Gurson parameters.

Card 13

This card gives number of group of distributed loads and number of concentrated loads. For displacement controlled loading these parameters are zero.

Card 14

This card is read only when first data in card 13 is non zero. This card provides data for each face.

Card 15

This card is read only when second data in card 13 is non zero. It provides data regarding node number and corresponding loads in x and y direction.

Card 16

Depending on the no. of group of loads and the number of groups of load fraction data is to be provided.

Card 17

Here the data represents no. of elements for which damage mechanics calculations is to be done.

Card 18

The data in this card represents the id of elements for which damage mechanics calculation is required.

Card 19

This card gives data regarding engineering quantity to be found (displacement, reaction etc.) and range of nodes for which it is to be found.

5.4 Running the MADAM Code

Input file was run using BARC in-house finite element code MADAM (Material Damage Modeling). MADAM has been developed based on the principles of continuum damage mechanics (Modified Gurson's model).

5.5 Post-processing of the output from MADAM code

1. .OUT: Gives the damage elements corresponding iteration number and gauss point and also confirms the input data.
2. MADAM-POST.OUT: Stores in detail the deformation history and different stress and strain values.
3. MADAM.DAT: Gives the displacement of each node and reaction of boundary nodes at specified interval.

5.6 Post-processing for load-ΔD and load-displacement

For RNTS, CT and TPB specimens the load-displacement values were given in MADAM.DAT file. A program Load-dia was used to find the load-displacement for all specimens and also load-ΔD value for RNTS specimen.

5.7 Post-processing for J-R curve

For calculating J-R values jcg code was used. There were two input files to the code, First 001JCG.INP file and second JCG.EXT file. In 001JCG.INP file there were data regarding total number of iterations and displacement and load corresponding to each iteration and

also data regarding the damage element corresponding gauss point and iteration number. JCG.EXT file contains data regarding specimen geometry and material properties. From out put file JCG.DAT we get J-R values and J_i (initiation) value.

CHAPTER 6

EVALUATION OF GURSON PARAMETERS

6.1 The effect of Gurson parameters on material behavior of SS 308L and SS 309L nuclear weld

The effect of Gurson parameters on load-ΔD (Diametrical contraction) & J-R curve is studied by varying one parameter at a time and keeping other parameters unchanged. In the study, two criteria were considered:

1. The sudden load dropping point in the RNTS load- ΔD curves
2. The slope of sudden load drop curve in the RNTS load- ΔD curves

Mean value of gurson parameter used in the study as initial parameter shown in table 6.1 below:

Gurson parameters	**Value**
Initial void volume fraction, f_o	0.00001
Critical void volume fraction, f_c	0.05
Final void volume fraction, f_f	0.2135
Void volume fraction at saturated nucleation, f_n	0.0055
Strain for nucleation, ϵ_n	0.1057
Standard deviation ,S_n	0.1
Modifying parameters q_1 q_2 q_3	1.5 1.0 2.25
Critical length parameter l_c	0.1
Modified ultimate void volume fraction f_u	0.566

Table 6.1 Initial Gurson parameters and their values

The Standard Deviation, Modifying Parameter, Critical length and Modified ultimate void volume fraction are constant gurson parameter, rest parameter are variable.

1. Results for SS 308L

The results of SS 308L for notch radius 2mm (R2) and notch radius 4mm (R4) is discussed below:

6.1.1 Variation of initial void volume fraction (f_0)

It represents the initial void fraction of the inclusions in the material which are not Strongly adhere to the matrix. It is determined by metallographic examination and calibrated by analysis of notched tensile test specimens.

The primary void portion of f_0, grows under increasing stress and strain of the material, while the inclusion part of the initial void volume fraction increases the probability of void nucleation.

Figure 6.1 and 6.2 shows the effect of f_0 for R2 and R4 respectively, on load dropping point for notched tensile specimens. With increase in values of f_0 there is increase in slope of load- ΔD curve as shown in table 6.2

.

1. **For notch radius 2mm (R2)**

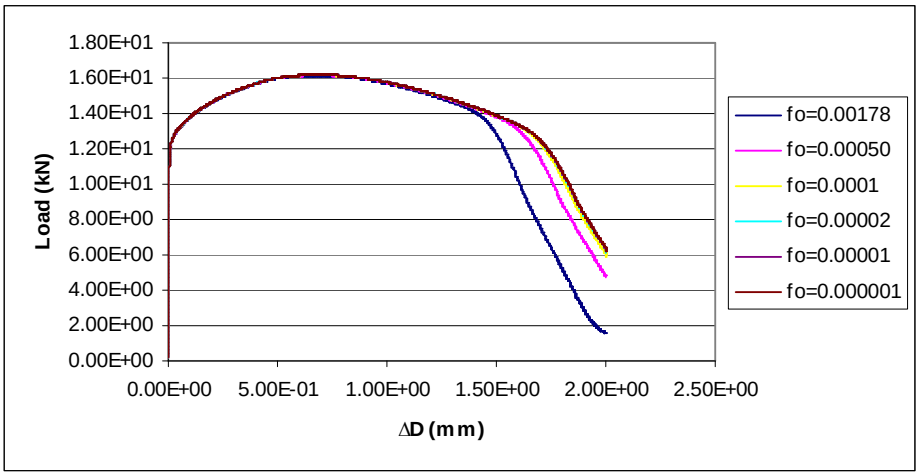

Fig 6.1 Load-ΔD curves for different f_o values of SS 308L R2

fo	ΔD at sudden load drop (mm)	Slope at sudden drop (kN/mm)
0.00178	1.55	25.96
0.0005	1.69	22.96
0.0001	1.71	21.67
0.00002	1.72	21.43
0.00001	1.74	21.92
0.000001	1.76	21.75

Table 6.2 ΔD and slope for different f_o values of SS 308L R2

2. **For notch radius 4mm (R4)**

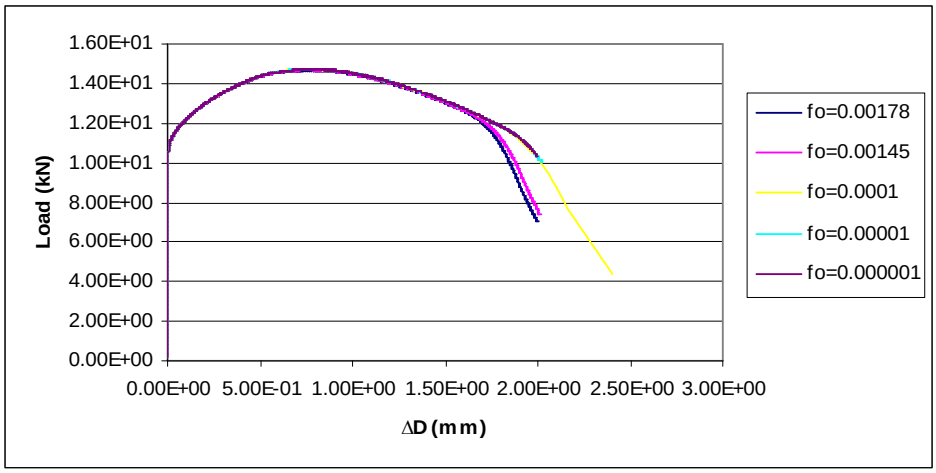

Fig 6.2 Load-ΔD curves for different f_o values of SS 308L R4

6.1.2 Variation of critical void volume fraction

The Critical void volume fraction (f_c) is the critical value of void volume fraction at which the material stress carrying capacity starts to decay more rapidly due to void coalescence. Lower f_c means that the material reaches this point earlier. The load dropping point in the load – diametric contraction curve is mainly influenced by this parameter. The figure 6.3 & 6.4 shows the load-ΔD curves for R2 & R4 respectively for different f_c values, as f_c value decrease, ΔD decrease while slope increase as in table 6.3.

1. **For notch radius 2mm (R2)**

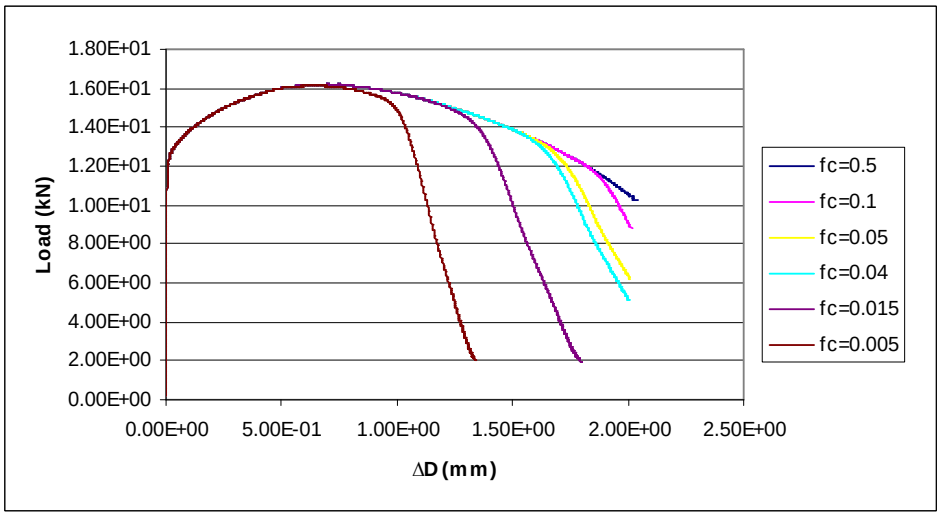

Fig 6.3 Load-ΔD curves for different f_c values of SS 308L R2

fc	ΔD at sudden load drop (mm)	Slope at sudden drop (kN/mm)
0.5	1.83	08.42
0.1	1.8	14.00
0.05	1.75	22.67
0.04	1.71	24.13
0.015	1.44	31.92
0.005	1.09	45.33

Table 6.3 ΔD and slope for different f_c values of SS 308L R2

2. For notch radius 4mm (R4)

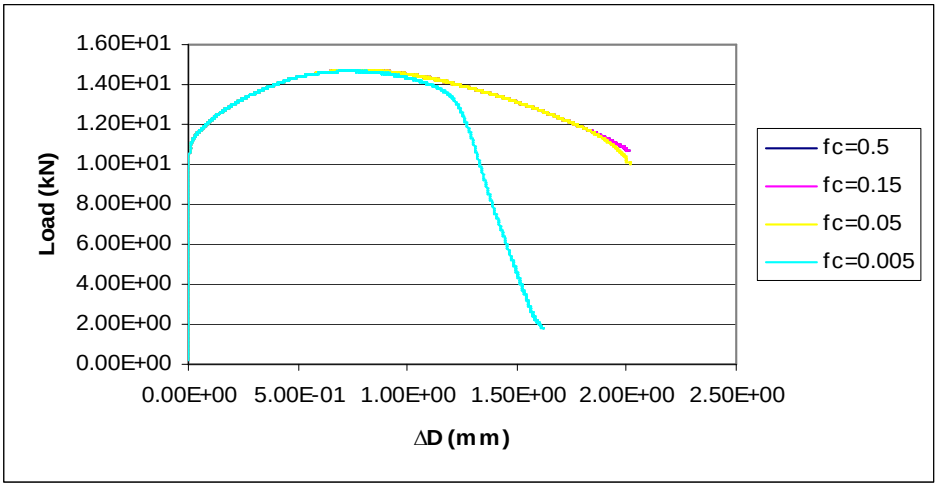

Fig 6.4 Load-ΔD curves for different f_c values of SS 308L R4

6.1.3 Variation of final void volume fraction

Final void volume fraction (f_f) is the actual void volume fraction associated with the complete loss of stress carrying capacity of the material matrix. Lower values of f_f force the material to loss the stress carrying capacity earlier and thus a steeper slope is obtained. The load dropping point remains unaffected by f_f, while the slope varies linearly. Figure 6.5 & 6.6 shows the variations of slope and (ΔD) diametrical contraction for different value of f_f for R2 & R4 respectively and table 6.4 shows the ΔD and slope at sudden load drop.

1. For notch radius 2mm (R2)

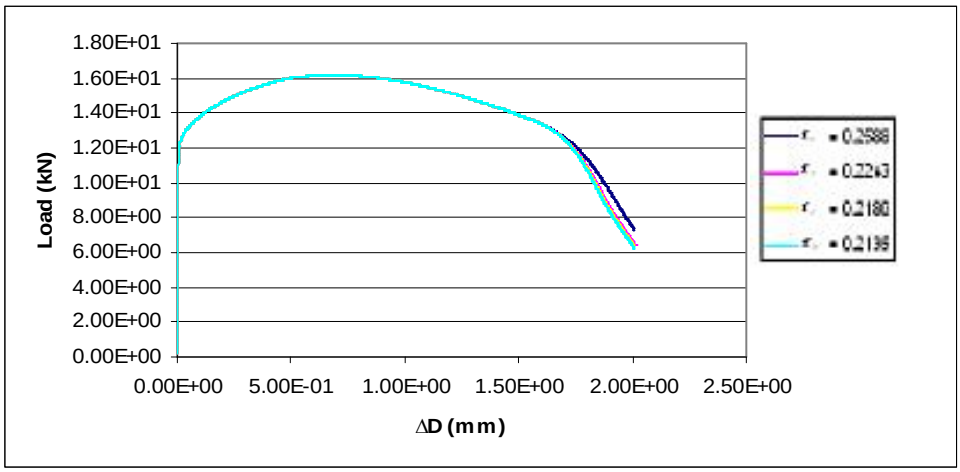

Fig 6.5 Load-ΔD curves for different f_f values of SS 308L R2

f_f	ΔD at sudden load drop (mm)	Slope of sudden drop (kN/mm)
0.2588	1.76	17.65
0.2243	1.75	22.22
0.218	1.74	22.31
0.2135	1.73	21.58

Table 6.4 ΔD and slope for different f_f values of SS 308L R2

1. **For notch radius 4mm (R4)**

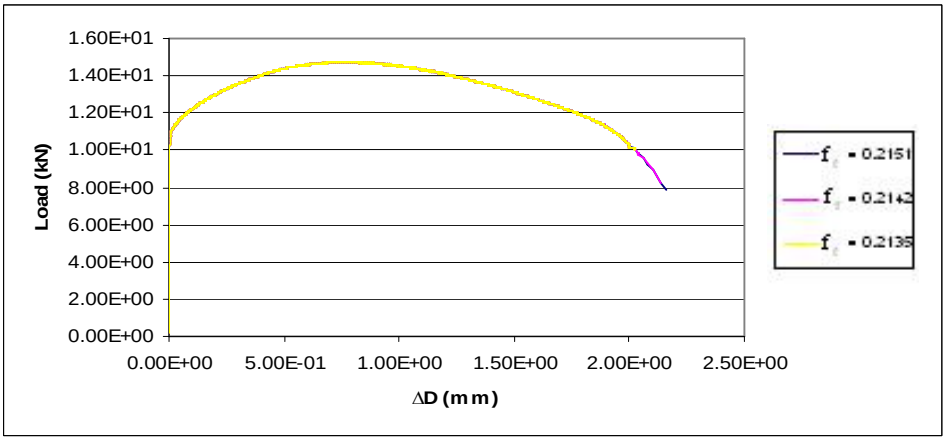

Fig 6.6 Load-ΔD curves for different f_f values of SS 308L R4

6.1.4 Variation of void volume fraction at saturated nucleation

Effect of void volume fraction at saturated nucleation is shown in figure 6.7 & 6.8 forR2

And R4 respectively, slope of Load- ΔD curve increases with increase in value of f_n and load dropping point decreases slightly as shown in table 6.5.

1. **For notch radius 2mm (R2)**

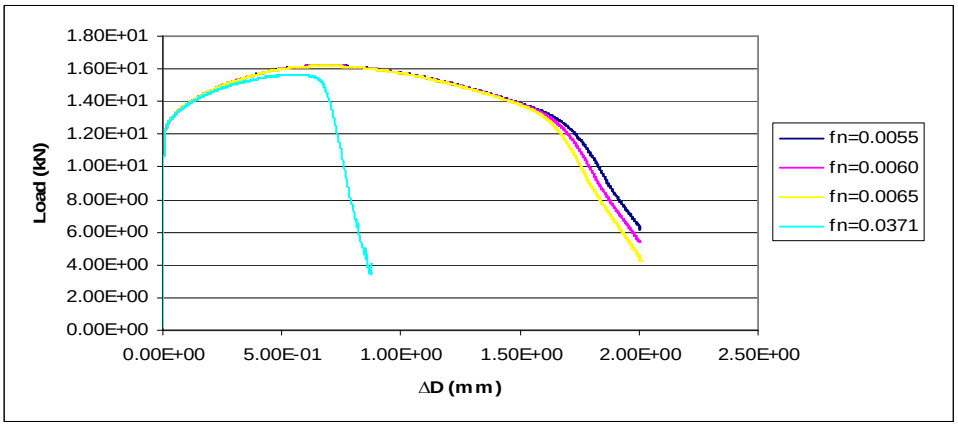

Fig 6.7 Load-ΔD curves for different f_n values of SS 308L R2

fn	ΔD at sudden drop (mm)	Slope at sudden drop (kN/mm)
0.0055	1.75	22.50
0.006	1.71	23.47
0.0065	1.68	24.50
0.0371	0.69	59.38

Table 6.5 ΔD and slope for different f_n values of SS 308L R2

2. **For notch radius 4mm (R4)**

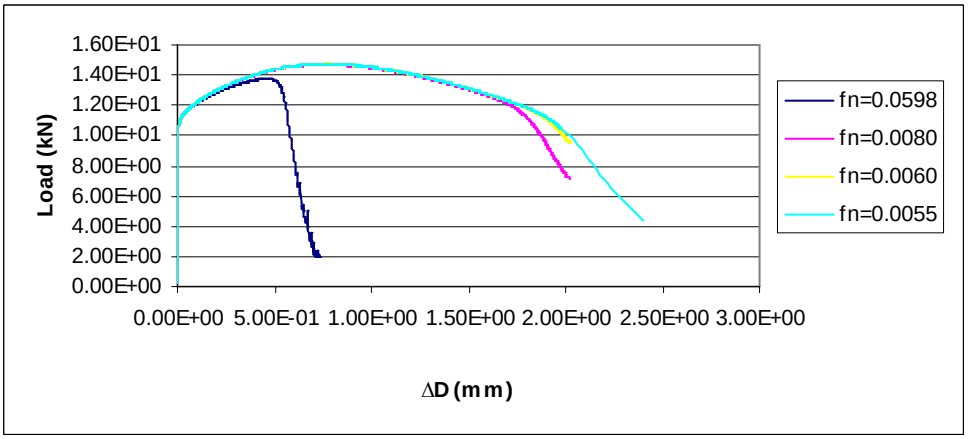

Fig 6.8 Load-ΔD curves for different f_n values of SS 308L R4

6.1.5 Variation of strain for nucleation

It is determined by conducting tensile tests & subsequent metallographic examination. The figure 6.9 & 6.10, below shows the effect of mean strain of void nucleation on load Dropping point for notched tensile specimens R2 & R4 respectively. With increase in values of ϵ_n there is decrease in slope of load- ΔD curve, as in table 6.6.

1. **For notch radius 2 (R2)**

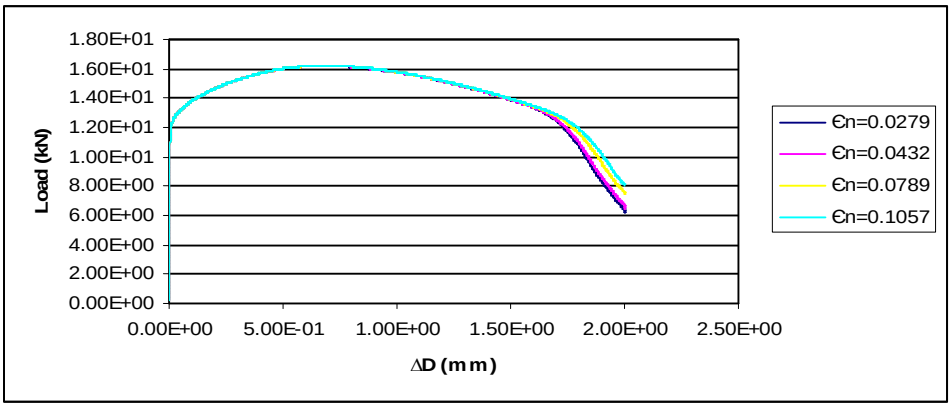

Fig 6.9 Load-ΔD curves for different ϵ_n values of SS 308L R2

ϵ_n	ΔD at sudden drop (mm)	Slope at sudden drop (kN/mm)
0.0279	1.72	21.11
0.0432	1.74	20.00
0.0789	1.77	19.30
0.1057	1.81	18.18

Table 6.6 ΔD and slope for different ϵ_n values of SS 308L R2

2. **For notch radius 4 (R4)**

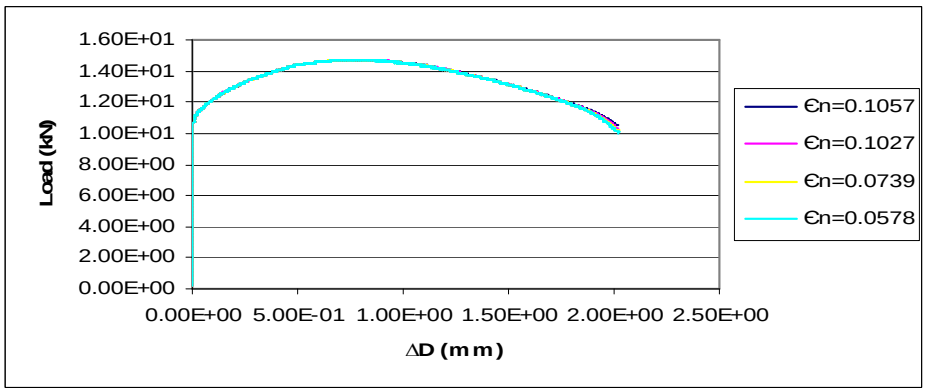

Fig 6.10 Load-ΔD curves for different ϵ_n values of SS 308L R4

2. Results for SS 309L

The results for SS 309L are shown in figure 6.11, 6.12, 6.13, 6.14 & 6.15 it's contain the graph's showing the load vs. ΔD for fo, fc, f_f, fn, & ϵ_n respectively at different values and table 6.7, 6.8, 6.9, 6.10 & 6.11 showing the diametrical contraction (ΔD**)** & slope at sudden load drop for different gurson parameter's fo, fc, f_f, fn, & ϵ_n respectively at different values.

The trends of variation of different gurson parameters at various values are same as in the case of SS 308L, so here only graphs and tables are shown for different gurson parameters. For detail descriptions consider the "Results for SS 308L" (above) for each gurson parameter.

6.1.6 Variation of initial void volume fraction

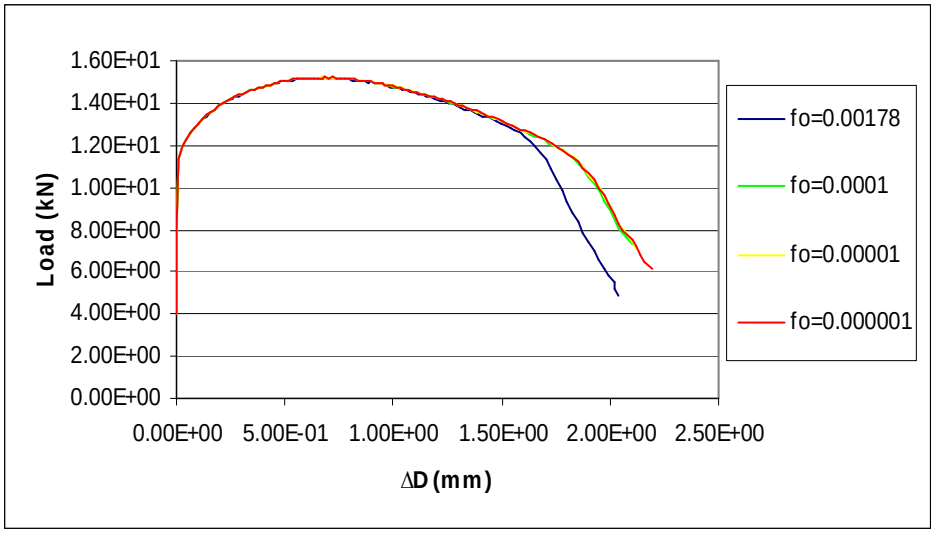

Fig 6.11 Load-ΔD curves for different f_o values of SS 309L

f_o	ΔD at sudden drops (mm)	Slope of sudden drop (kN/mm)
0.00178	1.65	19.98
0.0001	1.86	19.83
0.00001	1.88	19.54
0.000001	1.9	19.33

Table 6.7 ΔD and slope for different f_o values of SS 309L

6.1.7 Variation of critical void volume fraction

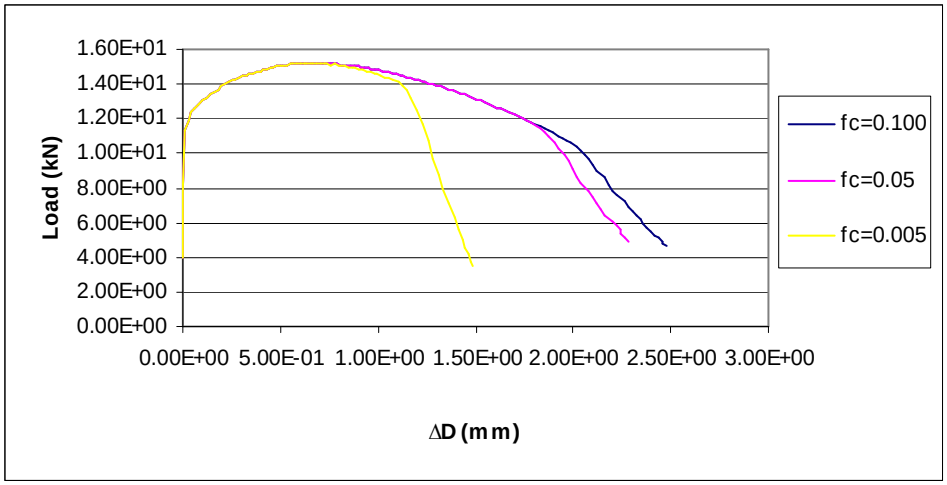

Fig 6.12 Load-ΔD curves for different f_c values of SS 309L

f_c	ΔD at sudden load drop (mm)	Slope of sudden drop (kN/mm)
0.1	2.04	13.33
0.05	1.88	16.90
0.005	1.15	33.62

Table 6.8 ΔD and slope for different f_c values of SS 309L

6.1.8 Variation of final void volume fraction

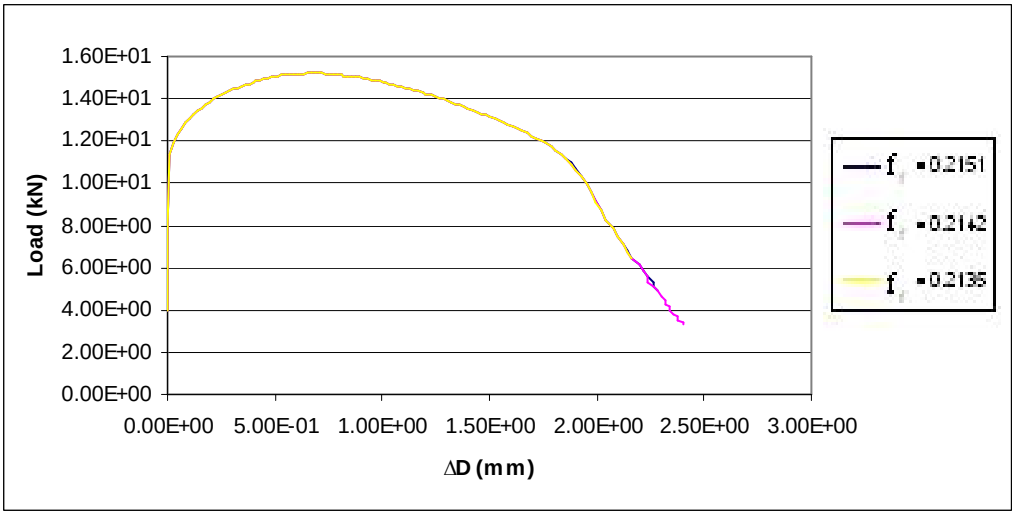

Fig 6.13 Load-ΔD curves for different f_f values of SS 309L

f_f	ΔD at sudden load drop (mm)	Slope of sudden drop(kN/mm)
0.2151	1.95	17.00
0.2142	1.95	18.00
0.2135	1.95	21.08

Table 6.9 ΔD and slope for different f_f values of SS 309L

6.1.9 Variation of void volume fraction at saturated nucleation

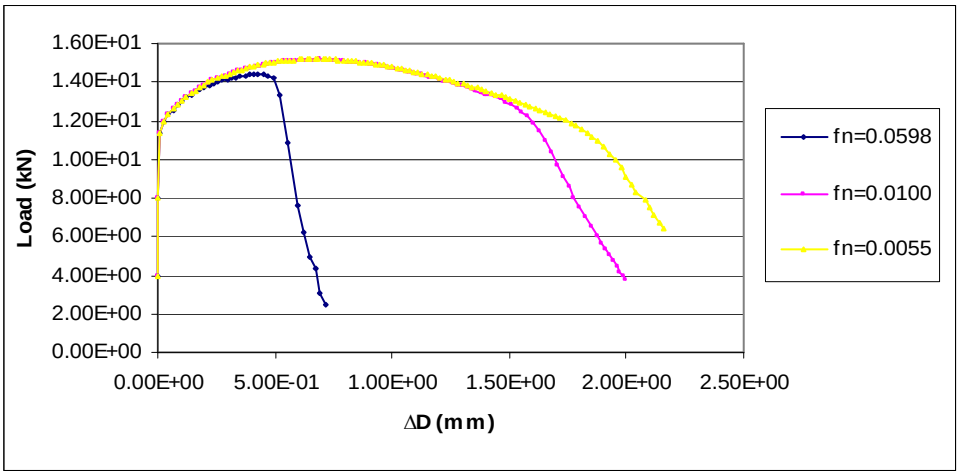

Fig 6.14 Load-ΔD curves for different f_n values of SS 309L

f_n	ΔD at sudden load drop (mm)	Slope of sudden drop (kN/mm)
0.0598	0.5	42.56
0.01	1.6	21.52
0.0055	1.9	16.84

Table 6.10 ΔD and slope for different f_n values of SS 309L

6.1.10 Variation of strain for nucleation

ϵ_n	ΔD at sudden drop (mm)	Slope of sudden drop (kN/mm)
0.1027	1.94	13.22
0.0739	1.9	14.62
0.0578	1.85	18.63

Table 6.11 ΔD and slope for different ϵ_n values of SS 309L

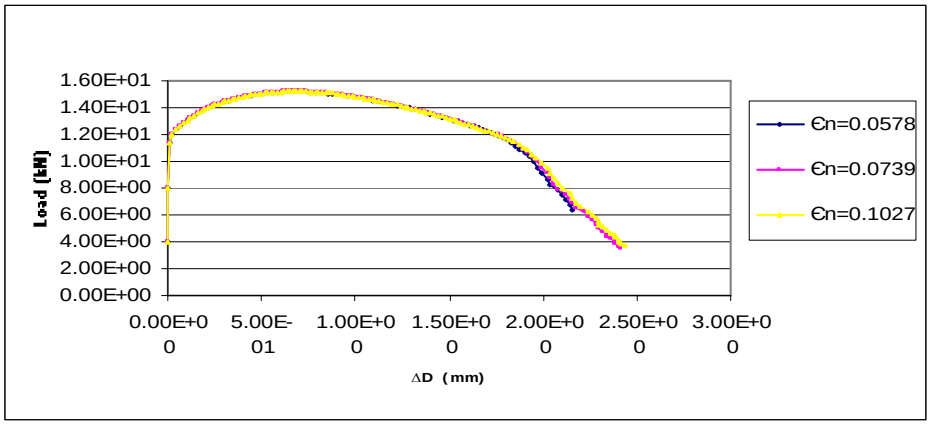

Fig 6.15 Load-ΔD curves for different Єn values of SS 309L

6.2 Determination of damage parameters from experimental and analytical load- ΔD curves

Effect of various damage parameters on Load-ΔD curve was studied in previous sections. Now the Gurson parameters for the SS 308L and SS 309L are to be found using experimental and analytical load- ΔD curves of RNTS R2 & R4 by curve fitting of analytical curve to experimental curve.

The selection criteria of the various Gurson parameters:

1. **Selection of fo:** Those value of fo, is selected for which the slope of sudden load drop is minimum and diametrical contraction (ΔD) is maximum.
2. **Selection of fc:** Those values of fc, is selected for which the slope of sudden load drop is minimum and ΔD is maximum.
3. **Selection of f_f:** There is little variation in this case so, any value can be selected.
4. **Selection of fn:** Those values of fn, is selected for which the slope of sudden load drop is minimum and ΔD is maximum.
5. **Selection of Єn:** Those values of Єn, is selected for which the slope of sudden load drop is minimum and ΔD is maximum.

6.2.1 Curve fitting of SS 308L RNTS R2

The experimental and analytical load- ΔD curves for different values of Gurson parameters is shown in figure 6.16.

Set of variable gurson parameters
f_o= 0.0001, f_c= 0.1, f_f= 0.2135, Єn = 0.1057, f_n= 0.0055.

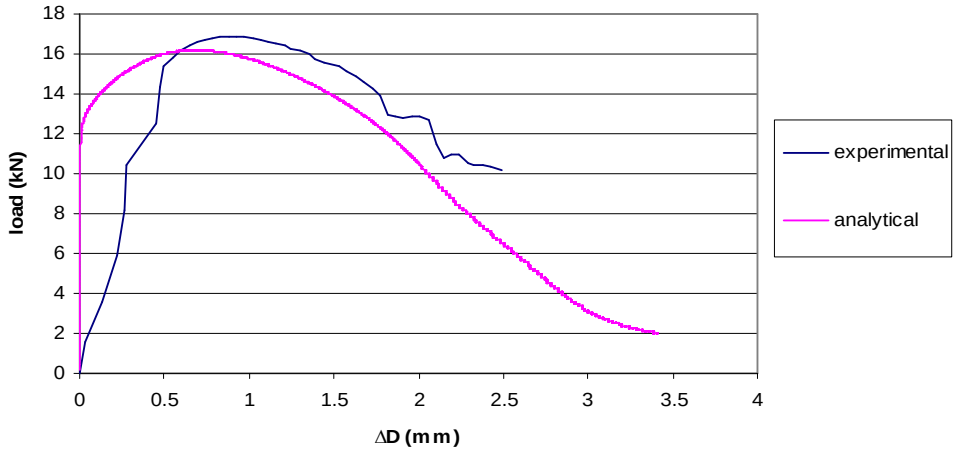

Fig 6.16 Experimental and Analytical load- ΔD curves for SS 308L R2

6.2.2 Curve fitting of SS 308L RNTS R4

The experimental and analytical load- ΔD curves for different values of Gurson parameters is shown in figure 6.17.

Set of variable gurson parameters
f_o= 0.00001, f_c= 0.1, f_f= 0.2151, Єn = 0.1027, f_n= 0.0060

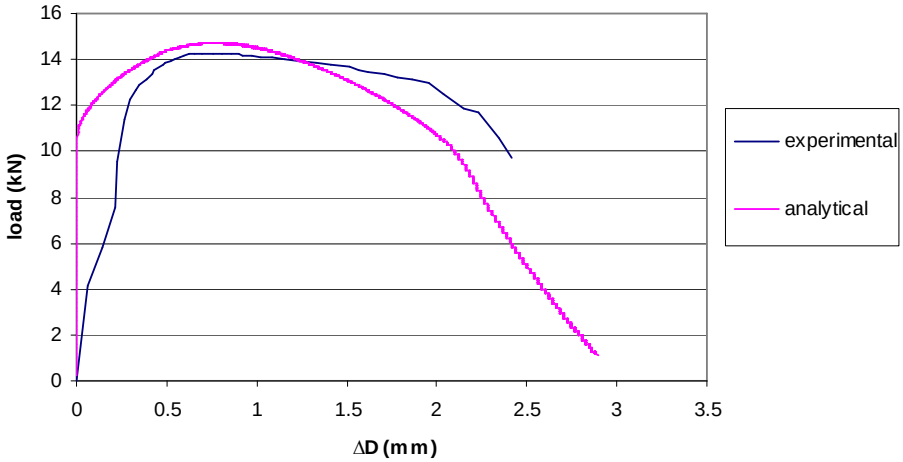

Fig 6.17 Experimental and Analytical load- ΔD curves for SS 308L R4

6.2.3 Curve fitting of SS 309L RNTS R4

The experimental and analytical load- ΔD curves for different values of Gurson parameters is shown in figure 6.18.

Set of variable gurson parameters
f_o= 0.000001, f_c= 0.1, f_f= 0.2151, Єn = 0.1057, f_n= 0.0055

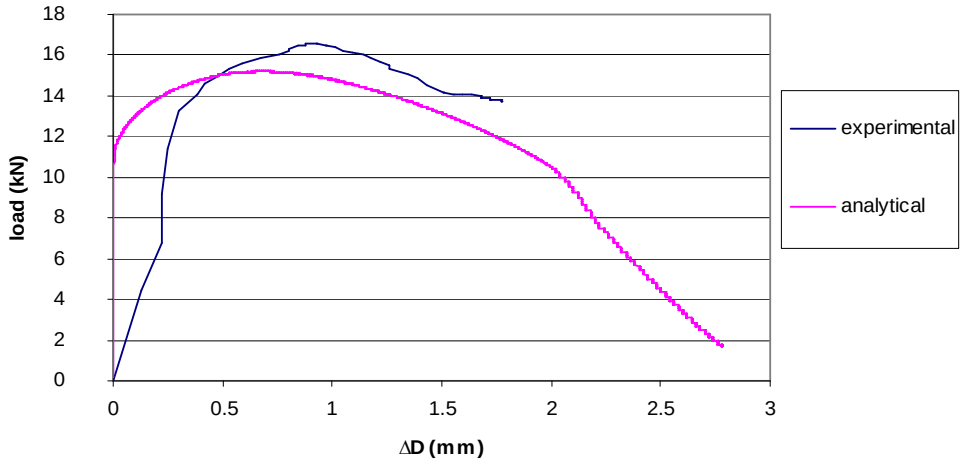

Fig 6.18 Experimental and Analytical load- ΔD curves for SS 309L R4

6.3 Comparative study of experimental and analytical J-R curves for CT specimen

The comparative study of experimental and analytical J-R curves for CT specimen, for fixed set of gurson parameter (obtained by the curve fitting of RNTS SS 308L & SS 309L, section 6.2, above), are done in this section and shown in figure 6.19.

The experimental and analytical curve is plotted and compared with respect to the J-initial values, slope of J-R curves and crack growth & J-value. As a result of comparisons, the set of gurson parameter is fixed for most matched experimental and analytical J-R curve.

The analytical J-R curve is plotted for those set of Gurson parameter, which were evaluated in section 6.2.1, 6.2.2, 6.2.3.

6.3.1 Comparison of J-R curve for SS 308L weld (R2& R4) CT specimen

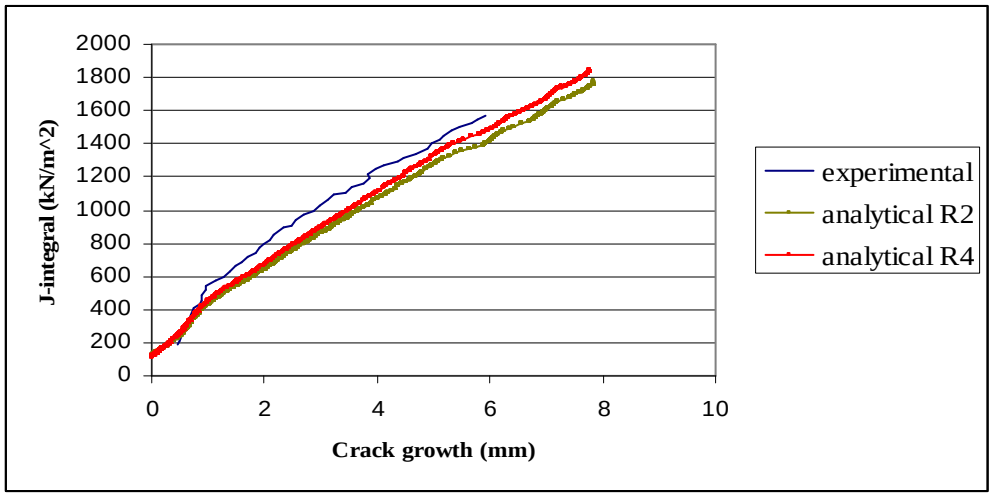

Fig 6.19 Experimental & analytical J-R curve for SS 308L (R2 & R4)

Discussion of Result:

Here the table (Table 6.12) below, for Crack growth, x1, x2, & x3 are shown in two parts:

Crack growth (mm)	(x1)	(x2)	(x3)
0.75	358.57	358.57	358.57
0.85	432	396	396
0.91	490	415.13	415.13
0.95	520	434.34	434.34
1.00	540	447	447
1.12	580	479	479
1.26	600	511.94	511.94
1.38	630	538	519
1.48	652	558	538.88
1.59	690	584.96	558.61
1.71	720	605.16	578.87
1.85	740	644.85	619.13
1.92	770	651	631.99
1.99	800	671.5	645.6
2.09	820	690.98	690.98
2.15	850	711.38	704.75
2.33	890	751	725.3
2.48	910	784	758.27
2.56	940	803.39	771
2.71	970	836.34	803.94
2.88	1000	869.57	844
2.99	1030	902.16	857.4
3.13	1060	921.7	889.21

3.23	1090	946.9	940.81
3.45	1110	992	959.4
3.56	1140	1017.54	972.34
3.76	1160	1082	1017.34
3.86	1190	1101.3	1042.95
3.96	1250	1130	1107.63
4.12	1270	1145	1132.79
4.35	1290	1183.72	1144.49
4.48	1320	1221.53	1169.32
4.67	1340	1258.85	1207.11
4.89	1370	1308.53	1244.07
4.98	1400	1320.87	1269
5.09	1430	1344.99	1293.23
5.19	1450	1369.22	1317.38
5.33	1480	1405.8	1332.5
5.45	1500	1418.06	1350.55
5.68	1530	1443.8	1381.5
5.79	1550	1457.26	1408.87
5.91	1570	1469.05	1417.24

Table 6.12 Experimental and Analytical data for SS 308L (R2 & R4)

Where,

X1 = Experimental value of J-integral

X2= Analytical value of J-integral for R4

X3= Analytical value of J-integral for R2

The table 6.13 for % error (below) is shown in two parts due to having too long:

% error (R4) = (x1-x2)/x1*100	% error (R2) = (x1-x3)/x1*100
0	0
8.33	8.33
15.27	15.27
16.47	16.47
17.22	17.22
17.41	17.41
14.67	14.67
14.60	17.61
15.45	18.35
15.22	19.04
15.95	19.60
12.85	16.33
15.45	17.92
16.06	19.30
15.73	15.73

16.30	17.08
15.61	18.50
13.84	16.67
14.53	17.97
13.77	17.11
13.04	15.60
12.41	16.75
13.04	16.11
13.12	13.68
10.63	13.56
10.74	14.70
6.72	12.29
7.45	12.35
9.60	11.38
9.84	10.80
8.23	11.27
7.45	11.41
6.05	9.91
4.48	9.19
5.65	9.35
5.94	9.56
5.57	9.14
5.01	9.96
5.46	9.96
5.63	9.70
5.98	9.10
6.42	9.72

Table 6.13 Percentage error for SS 308L (R2 & R4)

From the figure 6.19, table 6.12 and 6.13, it is observed that the analytical curve is the best matching with the experimental curve for SS 308L R4, as the maximum percentage error (17.4%) in case of SS 308L R4 is less than the maximum percentage of error (19.6%) in case of SS 308L R2, also the other value of % error is comparatively less for SS 308L R4.

So the best evaluated set of Gurson parameters for SS 308L from above conclusion is:

f_o= 0.00001, f_c= 0.1, f_f= 0.2151, Єn = 0.1027, f_n= 0.0060 ,q_1=1.5, q_2=1.0, q_3=2.25, S_n=0.1, f_u= 0.566.

6.3.2 Comparison of J-R curves for SS 309L buttering CT specimen

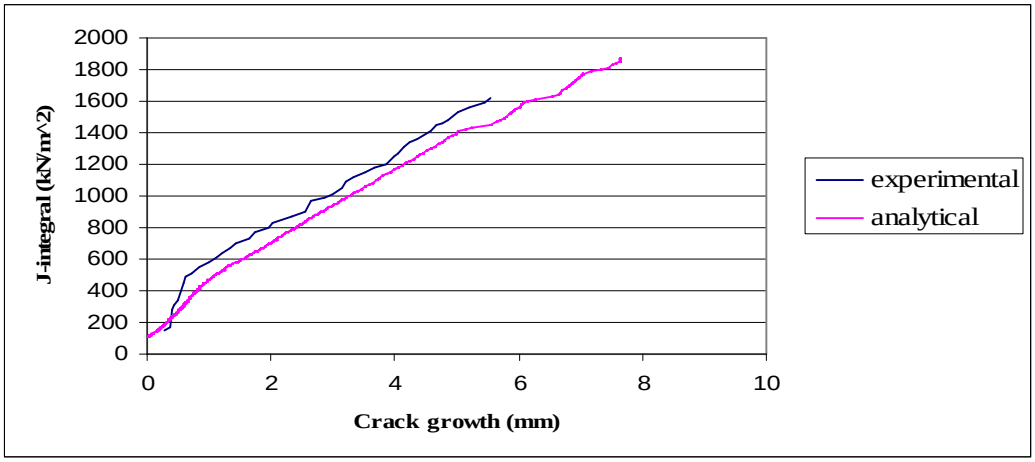

Fig 6.20 Experimental & analytical J-R curve for SS 309L R4

Discussion of Result:

From the figure 6.21 and table 6.14, it can be observed that the maximum percentage of error is around 20%, which is within the range of error. This % of error is varying from 5 to 20 % for various crack growth. For some value of crack growth the range of % of error is 15 to 20 % while for rest of the value of crack growth this range is from 5 to 15 %. So analytical and experimental J-R curve is matched correctly with some percentage of error within the range.

So the best evaluated set of Gurson parameters for SS 309L from above conclusion is:

f_o= 0.000001, f_c= 0.1, f_f= 0.2151, Єn = 0.1057, f_n= 0.0055 ,q_1=1.5, q_2=1.0, q_3=2.25, S_n=0.1, f_u= 0.566.

Crack growth (mm)	(y1)	(y2)	% error = (y1-y2)/y1*100
0.52	343	273.89	19.94868805
1.01	577	486.68	15.65337955
1.12	609	507.21	16.71428571
1.21	642	527.84	17.78193146
1.33	668	555.64	16.82035928
1.43	702	582.53	17.01851852
1.64	734	625.79	14.74250681
1.76	768	653.66	14.88802083
1.97	799	702.21	12.11389237
2.04	830	716.35	13.69277108
2.33	870	787.23	9.513793103
2.54	900	835.8	7.133333333

2.64	970	856.35	11.71649485
2.88	990	911.52	7.927272727
2.99	1010	939.93	6.937623762
3.16	1050	982.03	6.473333333
3.21	1090	988.95	9.270642202
3.33	1120	1016.22	9.266071429
3.53	1150	1058.8	7.930434783
3.67	1180	1097.67	6.977118644
3.86	1200	1139.1	5.075
3.98	1250	1166.38	6.6896
4.05	1270	1179.97	7.088976378
4.15	1310	1207.1	7.854961832
4.24	1340	1229.83	8.221641791
4.35	1360	1247.33	8.284558824
4.58	1410	1301.35	7.705673759
4.67	1450	1327.83	8.425517241
4.76	1460	1340.81	8.16369863
4.87	1480	1367.28	7.616216216
5.02	1530	1406.47	8.073856209
5.21	1560	1434.42	8.05

Table 6.14 Experimental, analytical & percentage error data for SS 309L

Where,
Y1= Experimental J-integral value for SS 309L R4
Y2= analytical J-integral value for SS 309L R4

6.4 Analytical J-R curves for TPB specimen for SS 308L and SS 309L

1st Set of variable gurson parameters
f_o= 0.0001, f_c= 0.1, f_f= 0.2135, Єn = 0.1057, f_n= 0.0055.

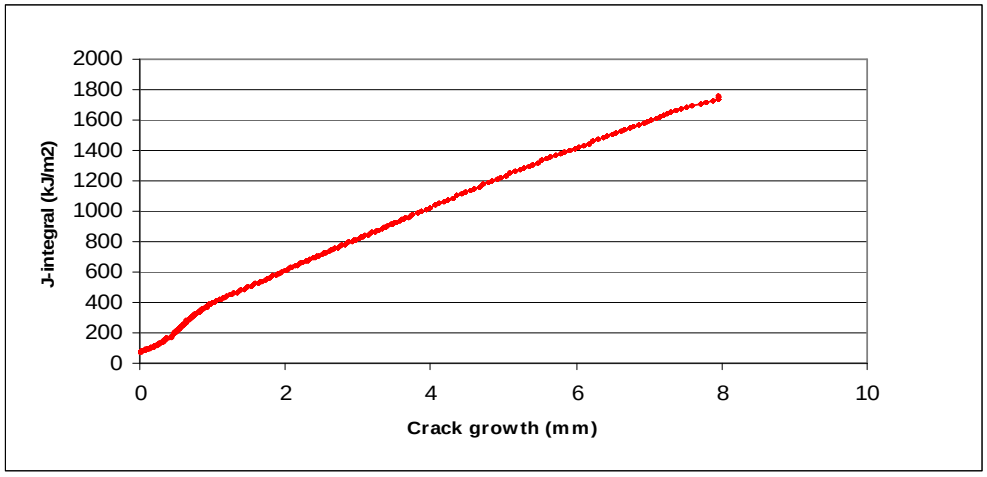

Fig 6.21 J-R curve for SS 308L R2 TPB

2nd Set of variable gurson parameters
f_o= 0.00001, f_c= 0.1, f_f= 0.2151, Єn = 0.1027, f_n= 0.0060

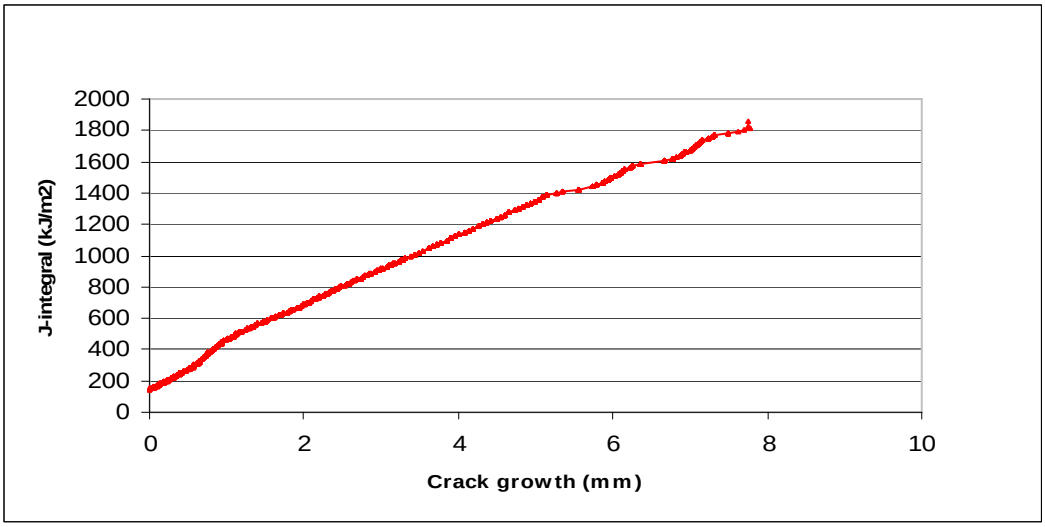

Fig 6.22 J-R curve for SS 308L R4 TPB

3rd Set of variable gurson parameters
f_o= 0.000001, f_c= 0.1, f_f= 0.2151, Єn = 0.1057, f_n= 0.0055

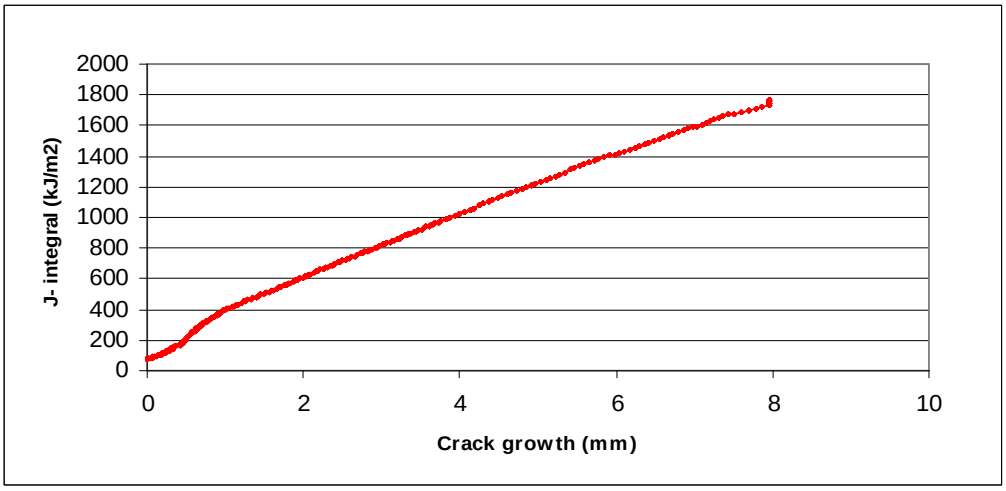

Fig 6.23 J-R curve for SS 309L R4 TPB

Here only the analytical study of the J-R curve for TPB specimen is done to predict the fracture characteristics of the material used in this thesis, because of the unavailability of the experimental data for J-integral and Crack growth for TPB specimen.

CHAPTER 7

CONCLUSIONS

The following conclusion can be stated from the present work:

1. It is confirm, from the comparison of the experimental and analytical results for J-R curves that the Gurson parameters are somewhat dependent of each other and it is possible to have several set of these Gurson parameters to describe the material behaviour simultaneously. The effect of different parameters on load –deflection curve of RNTS R2 & R4 for SS 308L and SS 309L is tabulated below.

Gurson parameters	The load dropping point in load- ΔD curve (RNTS specimen)	The final slope in load – ΔD curve (RNTS specimen)
fo	Yes	Slightly
fc	Yes (parabolic)	Very much (parabolic)
f_f	No	Yes (linear)
ϵ_n	Yes (linear)	Slightly
fn	Yes (linear)	Yes (linear)

Table 7.1 Effect of different Gurson parameters on load- ΔD & slope

2. The experimental and analytical J-R curve of CT-specimen have matched satisfactorily for the SS 308L R2 and R4, with respect to J-initial value (358.57 kj/m^2) and the slope of steady crack growth (slope of experimental J-R = 220 kj/m^2/mm), slope of analytical SS 308L R4 = 200, slope of analytical SS 308L R2 = 200).

3. From the comparative study of the experimental and analytical J-R curve of CT-specimen, it is observed that the analytical curve for SS 308L R4 is the best matching with the experimental curve, with respect to the maximum percentage of error as in case of SS 308L R4 it is less than the maximum percentage of error in case of SS 308L R2, also the other values of % error for each crack growth data is lesser for SS 308L R4.

4. From the comparative study of the experimental and analytical J-R curve for SS 308L R4 (CT) and SS 309L R4 (CT), it is observed that the maximum percentage of error in case of SS 309L (R4) CT- specimen is 19.94% at 0.52mm crack growth while the maximum percentage of error in case of SS 308L R4 is 17.4% at 1.12 mm crack growth, which is less than 19.94%. So the experimental and analytical J-R curve for SS 308L (R4) CT-specimen is matched more satisfactorily than the SS 309L R4 (CT). Also studying separately, it is found that the experimental and analytical J-R curves for SS 309L R4 (CT) match each other satisfactorily, as the maximum percentage of error in this case is 19.94%, which is within the general acceptance range of error (20%).
5. The analytical study of TPB specimen is done to predict the fracture characteristics of the SS 308L weld and SS 309L buttering material in nuclear weld.

Scope for future work

The Gurson model parameters that have been found out for SS 309L and SS 308L can be used to predict the fracture characteristics of the real components and should be tried to evaluate the fracture behaviour of real components. Similar studies can be done at higher temperatures and the Gurson material parameters can be evaluated for higher temperatures. The parametric studies with respect to variation of q1, q2 can be carried out to evaluate the effect of change in fracture characteristics with respect to q1 and q2.

REFERENCES

[1] **Chhibber, R; Arora, N; Gupta, S; Dutta, B. K.,** Use of bimetallic welds in nuclear reactors: associated problems and structural integrity assessment issues, Journal of Mechanical Engineering Science, Volume 220, Number 8, 1121-1133, 2006.

[2] **Wappling, D., Gunnars, J.,** and **Stahle, P**., Crack growth across a strength mismatched bimaterial interface, International Journal of Fracture, 89: 223–43, 1998.

[3] **Burstowm, M. C., Howard, I. C.** and **Ainsworth, R. A**., The influence of constraint on crack tip stress fields in strength mismatched welded joints, Journal of the Mechanics and Physics of Solids, 845–72, 1998.

[4] **Ranestad, Q., Zhang, Z.L.** and **Thaulow, C.** Quantification of geometry and material mismatch constraint in steel weldments with fusion line cracks, International Journal of Fracture, 99: 211–37, 1999.

[5] **Kim, Y.J., Kocak M, Ainsworth, R. A.** and **Zerbst, U.,** SINTAP defect assessment procedure for strength mismatched structures, Engineering Fracture Mechanics, 67: 529–46, 2000.

[6] **Kim, Y-J, Schwalbe, K-H** and **Ainsworth, R. A.,** Simplified *J*-estimations based on the Engineering Treatment Model for homogeneous and mismatched structures, Engineering Fracture Mechanics, 68:9–28, 2000.

[7] **Lee, H.** and **Kim, Y. J**., Interfacial crack-tip constraints and J-integrals in plastically mismatched bi-materials, Engineering Fracture Mechanics, 68: 1013–31, 2001.

[8] **Schwalbe K-H, Kocak M**, Editors. Mis-Matching of Welds, ESIS 17, London Mechanical Engineering Publications, 1994.

[9] **Schwalbe K-H, Kocak M**, Editors, Mis-Matching of Interfaces and Welds, GKSS-Forschungszentrum, Geesthacht; 1997.

[10] **R6: Assessment of the Integrity of structures containing defects**, British Energy Generation Report R/H/R6, Revision 4, 2001.

[11] **Schwalbe K-H, Zerbst U,** Engineering Treatment Model, International Journal of Pressure Vessel and Piping, 77:905–18. 2000.

[12] **Dsekmann, P., Pawliska, P.,** and **Richard, H. A**., Elastic plastic crack analysis under mixed mode loading conditions, International Journal of Fracture, 57:249-252. 1992.

[13] **Smith, R. N. L.,** Maximum principle stress, Engineering Fracture Mechanics, 26:463-469, 1987.

[14] **Waryznek, P.,** A two-dimensional crack propagation simulator. International Journal of Fracture, 6:281-304, 1991.

[15] **Finch, D. M.** and **Burdekin, F., M.**, Effects of welding residual stresses on significance of defects in various types of welded joint, Engineering Fracture Mechanics, 41 5 (1992), pp. 721–735.

[16] **Finch, D. M.**, Effects of welding residual stresses on significance of defects in various types of welded joint — II, Engineering Fracture Mechanics, 42 3, pp. 479–500, 1992.

[17] **M. K. Samal, Dutta B K, Kushwaha H S**, "Modelling of Ductile and Cleavage Fracture by Local Approach", BARC, E023, 2000.

[18] **M. K. Samal, Dutta B K, Kushwaha H S**, " 3-D Analysis of Piping Components using BARC Finite Element based Damage Mechanics Code MADAM", BARC,E023,2001.

[19] **S. Dhar, P. M. Dixit** and **R. Sethuraman, "**A continuum damage mechanics model for ductile fracture", International Journal of Pressure Vessels and Piping, Volume 77, Issue 6, May 2000, pp 335-344.

[20] **E. Schnack,** and **W. Weikl, "**Shape optimization under fatigue using continuum damage mechanics", Computer-Aided Design**,** Volume 34, Issue 12, October 2002, pp 929-938.

[21] **S Tarafder, V R Ranganath, S Sivaprasad** and **P Johri,** "Ductile fracture behaviour of primary heat transport piping material of nuclear reactors", Sadhana, Volume 28, part 1 & 2, February/April 2003, pp167–186.

[22] **J. Chattopadhyay , T.V. Pavankumar, B.K. Dutta, H.S. Kushwaha, "**Fracture experiments on through wall cracked elbows under in-plane bending moment: Test results and theoretical/numerical analyses", Reactor Safety Division, Hall-7, Bhabha Atomic Research Center, Mumbai, Engineering Fracture Mechanics, Volume 72,January 2005, pp 1461–1497.

[23] **Xiaosheng Gao, Tianhong Wang** and **Jinkook Kim, "**ductile fracture initiation toughness: Effects of void volume fraction, void shape and void distribution", International Journal of Solids and Structures, Volume 42, Issues 18-19, September 2005, pp 5097-5117.

[24] **V. Tvergaard** and **A. Needleman, "**Three dimensional micro-structural effects on plane strain ductile crack growth", International Journal of Solids and Structures, Volume 43, Issue 20, October 2006, pp 6165-6179.

[25] **M. Mashayekhi, S. Ziaei-Rad, J. Parvizian, J. Niklewicz** and **H. Hadavinia, "**Ductile crack growth based on damage criterion: Experimental and numerical studies", Mechanics of Materials**,** Volume 39, Issue 7, July 2007, pp 623-636.

[26] **A. Abou-Chakra Guéry, F. Cormery, J.F. Shao** and **D. Kondo, "**micromechanical model of elastic-plastic and damage behavior of a cohesive geometrical", International Journal of Solids and Structures, In Press, Corrected Proof, October 2007.

[27] **T.V.Pawan Kumar, J Chattopadhyay, Dutta B.K** & **Kushwaha H.S**, "Study of Crack Tip and Transfer of parameter in 2-D geometry", BARC, E031, 1998.

[28] **George E.Dieter**, "Mechanical Metallurgy", university of Maryland, TMH.